A&A manuscript no.
(will be inserted by hand later)

Your thesaurus codes are:
06(02.01.3; 02.12.1; 06.01.1; 08.01.1)

ASTRONOMY
AND
ASTROPHYSICS
21.8.1995

The solar iron abundance: not the last word

R.I. Kostik[1], **N.G. Shchukina**[1], **and R.J. Rutten**[2]

[1] Main Astronomical Observatory, National Academy of Sciences, 252650 Kiev-22, Ukraine
[2] Sterrekundig Instituut, Postbus 80000, NL–3508 TA Utrecht, The Netherlands

Received date; accepted date

Abstract. Determinations of the solar iron abundance have converged to the meteoritic value with the Fe II studies of Holweger et al. (1990), Biémont et al. (1991) and Hannaford et al. (1992) and the Fe I results of Holweger et al. (1991). However, the latter authors pointed out that Blackwell et al. (1984) obtained a discordant result from similar oscillator strengths. A recent debate on this lingering discrepancy by the Oxford and Kiel contenders themselves has not clarified the issue. We do so here by showing that it stems from systematic differences between equivalent widths and oscillator strengths which masquerade as difference in fitted damping enhancement factors.

We first discuss the various error sources in classical abundance determination and then emulate both sides of the debate with abundance fits of our own. Our emulation of the Oxford side shows that the abundance anomaly claimed by Blackwell et al. (1984) for solar Fe I 2.2 eV lines vanishes when equivalent width measurements from other authors are combined with better evaluation of the collisional damping parameter.

On the Kiel side, we find that the oscillator strengths of Bard et al. (1991) used by Holweger et al. (1991) produce a suspicious trend when used to fit solar Fe I lines, whereas comparable application of oscillator strengths from Oxford does not. The trend is mainly set by categories of Fe I lines not measured at Oxford; for lines of overlap the two sets agree and deliver the iron abundance value $A_{\rm Fe} = 7.62 \pm 0.04$ which exceeds the meteorite value. The dissimilar lines may suffer from solar line-formation effects.

We conclude that the issue of the solar iron abundance remains open. Definitive oscillator strengths are still needed, as well as verification of classical abundance determination by more realistic representations of the solar photosphere and of photospheric line formation.

Key words: Atomic data – Line: formation – Sun: abundances – Stars: abundances

1. Introduction

The solar iron abundance represents a fundamental quantity of cosmochemistry that is much debated in the literature. In 1991, the determinations by Holweger et al. (1991) and Biémont et al. (1991) appeared to lay the debate to rest. Their results were from Fe I lines and Fe II lines, respectively, utilized reliable lifetime calibrations, agree quite closely, and also agree very well with the C I chondrite meteoritic value. Indeed, the latter authors were sufficiently confident of their result to call their paper in its title "a final word!" on the solar iron abundance. However, the former authors pointed out in their discussion that puzzling discrepancies remain that are not easily explained. The latter form the topic of this paper.

Upon submission we were informed by the referee of the existence of other manuscripts on these discrepancies, in which these are debated by the principal contestants (Blackwell et al. 1995, Holweger et al. 1995). Thanks to mediation by referee and editor, we have been able to take these manuscripts into account before their appearance. They enable us to pinpoint the nature of the discrepancies in Sect. 5 by taking a third-party point of view.

We need to emphasize at the outset of this paper that these discrepancies are not the only cloud on the horizon of solar iron abundance determination. The papers quoted above adhere strictly to the narrow constraints of classical modeling, adopting plane-parallel and LTE line formation. The Sun's actual complexity as well as many atomic physics uncertainties are simply accounted for by adopting an error-correcting one-dimensional model atmosphere (cf. Rutten & Kostik 1982), by fitting observed spectral lines with the ad-hoc parameters provided by micro- and macroturbulence and damping enhancements, and by the assumption of a normal error distribution which permits straightforward averaging over lines with the rms variation taken as precision indicator. Even in the absence of internal discrepancies, this edifice of classical abundance determination is built on shaky ground as long as its tractability assumptions are not verified by detailed modeling (see the excellent review by Gustafsson & Jørgensen 1994). We return to this issue in Sect. 6, but restrict ourselves in the meantime to the classical assumptions as if we may take them all for granted—notwithstanding our earlier cooperations where we emphatically did not (Rutten & Kostik 1982, 1988, Shchukina et al. 1990, Bruls et al. 1992, Carlsson et al. 1992, 1994). Thus, in this paper we join the game played currently by Blackwell et al. (1995) and Holweger et al. (1995), in which the rules limit the debate to (blaming one another's) choice of microturbu-

Send offprint requests to: R.I. Kostik

lence, damping enhancements, photospheric model, equivalent width measurements or use of weak versus strong lines, in order to find out whose Fe I transition probabilities are the better ones and whether the solar iron abundance is "high" or "low" (i.e., higher than or equal to the meteorite value). However, we do add a new tactic by independent numerical emulation of the contenders' input data, codes, and results.

During the 1980's solar iron abundance studies were dominated by the advent of new oscillator strengths from Oxford (e.g., Blackwell et al. 1979, 1980, 1982a, 1982b, 1982c, 1984, 1986). In principle, these did away with one free parameter, the bound-bound transition probability or *gf*-value; in practice, they mostly concerned strong lines in the (ultra-)violet whereas abundance determiners rely on weaker lines at less crowded longer wavelengths. The Oxford scale was extended to the latter lines through empirical solar-spectrum fitting by Gurtovenko & Kostik (1981, 1982, 1989), Rutten & van der Zalm (1984) and Thévenin (1989). With the Oxford absolute scale, the solar iron abundance converged to a value near $A_{\rm Fe} = 7.65$, where $A_{\rm Fe}$ (called A below) is defined on the usual logarithmic difference scale by $A_{\rm Fe} = \log(n_{\rm Fe}/n_{\rm H}) + 12$ with $n_{\rm Fe}/n_{\rm H}$ the number density ratio of iron particles to hydrogen particles. Blackwell et al. (1984) obtained $A_{\rm Fe} = 7.67 \pm 0.02$, Gurtovenko & Kostik (1989) $A_{\rm Fe} = 7.64 \pm 0.03$, Rutten & van der Zalm (1984) $A_{\rm Fe} = 7.63 \pm 0.04$; Anders & Grevesse (1989) recommended $A_{\rm Fe} = 7.67$. This value is 45% higher than the meteoritic result $A_{\rm Fe} = 7.51 \pm 0.01$ (Anders & Grevesse 1989, cf. Booth 1989).

The 1990's started with divergence when Holweger et al. (1990) derived $A_{\rm Fe} = 7.48 \pm 0.09$ from Fe II lines whereas Pauls et al. (1990) used three Fe II lines to obtain $A_{\rm Fe} = 7.66 \pm 0.06$. The Fe II analysis of Biémont et al. (1991) then supplied the (or perhaps their) "final word" as $A_{\rm Fe} = 7.54 \pm 0.03$. It was nicely confirmed by the companion paper of Holweger et al. (1991), giving $A_{\rm Fe} = 7.50 \pm 0.07$ from *gf*-values of Fe I lines measured by Bard et al. (1991), and again by the additional Fe II measurements of Hannaford et al. (1992) which yield $A_{\rm Fe} = 7.48 \pm 0.04$ and, specifically, $A_{\rm Fe} = 7.54 \pm 0.06$ for just the three lines of Pauls et al. (1990). These values agree comfortably well with the meteoritic value.

However, Holweger et al. (1991) drew attention to a puzzling difference between their results and the earlier Oxford ones. The *gf* values of Bard et al. (1991) agree rather well with the Oxford values for the lines of overlap, differing by only 0.034 dex on average. This offset is much too small to explain the 0.17 dex difference between the two resulting abundance values. For the rest the two analyses are quite similar; Holweger et al. (1991) commented that the major difference is in the choice of the microturbulence but that this explains only an additional 0.05 dex. Thus, the puzzle is that the results of Blackwell et al. (1984) and of Holweger et al. (1991) differ much more than their input, without clear reason. This discrepancy is the main topic of this paper, as it is also for Blackwell et al. (1995) and Holweger et al. (1995) who after extensive reanalysis come up once more with a "high" ($A_{\rm Fe} = 7.63$) and a "low" ($A_{\rm Fe} = 7.51 \pm 0.05$) value, respectively, but no convincing explanation of the difference. The recent paper of Milford et al. (1994) adds evidence for a low value ($A_{\rm Fe} = 7.54 \pm 0.05$) but does not solve the discrepancy either.

Another discrepancy discussed below, in this case put forward from Oxford (Blackwell et al. 1982c, Blackwell et al. 1984), is the possibly anomalous behavior of lines from multiplets 62 and 64 with lower excitation energy near 2.2 eV. The Oxford group found that these are best reproduced with iron abundance values that are lower by 0.06 dex on average than for the other lines in their sample. Others have disagreed (Kipper 1987, Babii & Kovalchuk 1988, Holweger et al. 1991), and it is not the same anomaly as the one in the curve of growth results of Rutten & Zwaan (1983) although Blackwell et al. (1984) claim so; the latter dip is much larger and is due to errors in the equivalent widths of Moore et al. (1966) as demonstrated by Rutten & van der Zalm (1984). However, a 2.2 eV dip similar to the Oxford solar one was also obtained for two metal-deficient stars by Magain (1984). He suggested that it may be due to the fact that the corresponding Fe I levels ionize to unusually high levels of Fe II that differ between the upper and lower levels of the 2.2 eV lines.

The organization of this paper is as follows. In the next section, we follow the example of Holweger et al. (1991) and discuss results for just the four lines of overlap between their analysis and the one of Blackwell et al. (1984). These serve to show that larger samples should be studied. We then do so, detailing the method and input in Sect. 3. We first quantify various error sources in Sect. 4 in general for a larger sample and then extend the results in Sect. 5 with lines from both sides to address the above discrepancies. New lines and new comparisons were added to this section after we got hold of the manuscripts by Blackwell et al. (1995) and Holweger et al. (1995); these enable us to pinpoint the nature of the high-low discrepancy as a suspicious-looking trend produced in abundance values when using the oscillator strengths of Bard et al. (1991). In Sect. 6 we discuss its causes and make clear that this paper isn't the last word yet. We conclude the paper in Sect. 7.

This paper continues a research program for determining oscillator strengths and abundance values from the optical solar spectrum at Kiev that was founded and led during many years by Prof. Ernest A. Gurtovenko, as was the cooperation between our institutes at Kiev and Utrecht. He died at Kiev on January 20, 1994. We dedicate this paper to his memory.

2. Initial tests

Henceforth we denote the input parameters and results of the group led by Blackwell as "Oxford" and those used by Holweger and coworkers as "Kiel" (although the *gf* values actually are from Hannover); our own results are marked by "Kiev". There are only four lines of overlap between the lists of Blackwell et al. (1984) and Holweger et al. (1991); they are specified in Table 1. The first one (Fe I 608.27 nm) is from multiplet 64 and belongs to the anomalous 2.2 eV lines; Holweger et al. (1991, 1994) find it behaves normally. The columns specify per line the wavelength λ in nm and, for Kiel and Oxford respectively, the equivalent width W in pm, the logarithm of the *gf* value, and the corresponding iron abundance value A on the logarithmic H = 12 scale.

The bottom line specifies the average abundance derived from the four lines. At Kiel, the latter resulted from fitting the observed W's with microturbulence $v_{\rm mi} = 1.0\,{\rm km\,s^{-1}}$ and collisional damping enhancement factor $E = 2.0$, whereas the Oxford group choose $v_{\rm mi} = 0.845$ and let E vary with excitation energy, using $E = 1.2$ for these four lines. The bottom line of Table 1 shows that the resulting mean abundances from Kiel and Oxford differ by 0.11 dex, indeed far in excess of the

mean difference $\Delta \log gf \approx 0.01$ dex. Apart from the values of W, $\log gf$, $v_{\rm mi}$ and E used by the two groups there should be no other differences since the same model of the photosphere (Holweger & Müller 1974) was used with the same formalisms to derive iron abundance values by fitting observed equivalent widths.

Table 1. Input data and results from Kiel and Oxford for the four lines of overlap

	Kiel	Kiel	Kiel	Oxford	Oxford	Oxford
λ [nm]	W	$\log gf$	A	W	$\log gf$	A
608.27	2.82	−3.59	7.48	3.40	−3.57	7.607
675.01	7.70	−2.61	7.60	7.58	−2.62	7.655
694.52	8.20	−2.44	7.50	8.38	−2.48	7.658
697.88	7.90	−2.48	7.54	8.01	−2.50	7.655
$\overline{A}$			7.53			7.644

Table 2. Kiev emulations for the lines of Table 1

gf	Kiel	Kiel	Kiel	Kiel	Oxf.	Oxf.
W	Kiel	Kiel	Oxf.	Kiel	Kiel	Oxf.
E	Kiel	Kiel	Kiel	Oxf.	Kiel	Oxf.
$v_{\rm mi}$	Kiel	Oxf.	Kiel	Kiel	Kiel	Oxf.
λ [nm]						
608.27	7.481	7.492	7.605	7.484	7.461	7.606
675.01	7.595	7.655	7.574	7.640	7.605	7.689
694.52	7.497	7.564	7.537	7.552	7.537	7.697
697.88	7.538	7.599	7.561	7.584	7.558	7.692
$\overline{A}$	7.528	7.578	7.569	7.565	7.540	7.671

We test the effects of the parameter differences one by one in Table 2, using a code (henceforth the "Kiev" code) developed by Gadun & Sheminova (1988) to fit the Kiel input data (results in second column), the Oxford input data (last column), and four sets in which one of the Kiel parameters is replaced by the Oxford value as indicated. The results are, averaged over the four lines:

- decrease of the Kiel microturbulence $v_{\rm mi} = 1.0\,{\rm km\,s^{-1}}$ to the Oxford value $v_{\rm mi} = 0.845\,{\rm km\,s^{-1}}$ gives a mean abundance increase $\Delta A = 0.050$ dex (columns 2 and 3);
- adopting the Oxford equivalent widths W increases the abundance by $\Delta A = 0.041$ dex (columns 2 and 4);
- reducing the damping enhancement factor E from 2.0 to 1.2 gives $\Delta A = 0.037$ dex (columns 2 and 5);
- the gf differences cause $\Delta A = 0.012$ dex (columns 2 and 6);
- inconsistencies between the computer codes used at Oxford and Kiel produce $\Delta A = -0.027$ dex.

The last result follows from comparing the fourth and seventh columns of Table 1 with the corresponding second and last columns of Table 2, respectively giving the Kiel and Oxford results and our Kiev emulations. The Kiev code reproduces the Kiel results to well within 0.01 dex, in keeping with the minute difference in city name. In contrast, the Oxford emulations obtained with the Kiev code differ by over 0.03 dex from the actual Oxford results for three of the four lines. Thus, there are inconsistencies between the Kiev and Oxford codes that presumably hold similarly between the Kiel and Oxford codes.

The sum of these five differences $\Delta A = 0.050 + 0.041 + 0.037 + 0.012 - 0.027 = 0.113$ dex identifies the four-line average difference between Kiel and Oxford as due to a combination of differences in the four input parameters $v_{\rm mi}$, W, E and $\log gf$ and additional code inconsistencies. The latter partially cancel the effect of the former.

Given the assumptions of LTE, horizontal homogeneity and the Holweger-Müller model photosphere, explanation of this difference within the constraints of classical abundance determination requires further scrutiny of the four input parameters, as done at length by Blackwell et al. (1995) and Holweger et al. (1995) and once more by us below. An additional issue is set by the apparent Kiev–Oxford and Kiel–Oxford code inconsistencies. They produce Kiev–Oxford differences of up to $\Delta A = 0.039$ dex (Fe I 694.52 nm), large enough to require further inspection.

Table 3. Input data and tests for the 22 Kiel lines

λ [nm]	E.P.	$\log gf$	ΔA codes	ΔA BD–W	ΔA U–W
521.73	3.21	−1.07	0.01	0.004	0.031
532.41	3.21	−0.10	0.02	0.004	0.031
539.31	3.24	−0.72	0.02	0.004	0.028
540.57	0.99	−1.88	0.03	0.020	−0.132
543.45	1.01	−2.11	0.02	0.020	−0.115
558.67	3.37	−0.10	0.02	0.001	0.023
570.15	2.56	−2.13	0.01	0.020	−0.018
577.84	2.59	−3.44	0.01	0.001	−0.001
578.46	3.40	−2.53	0.01	0.000	0.002
608.27	2.22	−3.59	0.00	−0.003	−0.005
624.06	2.22	−3.23	0.00	−0.008	−0.013
624.63	3.60	−0.73	0.01	0.007	0.024
630.15	3.65	−0.72	0.01	0.002	0.020
639.36	2.43	−1.43	0.01	0.060	−0.044
640.00	3.60	−0.29	0.02	0.009	0.037
641.16	3.65	−0.60	0.01	0.008	0.027
642.13	2.28	−1.94	0.00	−0.014	−0.086
658.12	1.48	−4.68	0.00	0.000	0.000
673.95	1.56	−4.79	0.00	0.000	0.000
675.01	2.42	−2.61	0.00	−0.007	−0.038
694.52	2.42	−2.44	0.00	−0.005	−0.039
697.88	2.48	−2.48	0.00	−0.004	−0.040

3. Input data and method

We extend our tests to larger samples by running emulations on all 22 "Kiel" lines given in Table 1 of Holweger et al. (1991) and all 25 "Oxford" lines in Table 1 of Blackwell et al. (1984). We also employ a compilation of 19 selected Oxford lines, including 13 lines from other Oxford publications that are specified underneath Table 4. These lines were chosen to obtain an Oxford selection that is comparable to the 22 Kiel lines in their equivalent width and wavelength coverage. Unfortunately, the similarity breaks down for excitation energy because of the lack of high-excitation lines in the Oxford measurements; there are none above 3 eV. These three sets of lines are specified by their wavelengths in Tables 3–5 where the columns E.P. denote lower-level excitation potential in eV. In addition, we use lines from the manuscripts of Blackwell et al. (1995) and Holweger et al. (1995) in Sect. 5.3, in the line lists given in Tables 8 and

9. Finally, in Figs. 8–9 we show results from Gurtovenko & Kostik (1989) for 731 Fe I lines and 62 Fe II lines, respectively.

The Kiel and Oxford line lists also contain W values used below; in addition, we employ equivalent widths determined by Rutten & van der Zalm (1984) and Gurtovenko & Kostik (1989), and new measurements from the Jungfraujoch Atlas (Delbouille et al. 1973) following the recipes of Gurtovenko & Kostik (1989). They are specified in Tables 4, 5, 7–9.

Following the Oxford and Kiel examples, we adopt the model photosphere of Holweger & Müller (1974) and assume LTE. We have checked the Kiev code of Gadun & Sheminova (1988) used here by comparing it with an unpublished code written by one of us (Shchukina). The two codes differ primarily in their evaluations of the continuous opacity, the latter code giving opacities that are larger by 4–5%. The differences that result between abundance fits with the two codes for the 22 Kiel lines remain below 0.005 dex, except for one line which reaches 0.015 dex. Thus, the two codes agree very well.

A similar comparison is detailed in the third column of Table 3 in which ΔA(codes) stands for the differences in fitted abundance A between the Kiel and Kiev results when the Kiel input values and parameters are used with the Kiev code. The average Kiev–Kiel difference is 0.01 dex; only one line reaches $\Delta A = 0.03$ dex.

These comparisons give us confidence that the Kiev code may serve as a benchmark facility. In the next section it is employed to quantify the effect of changes in the various input parameters and assumptions of classical abundance determination for the 22 Kiel lines.

4. Uncertainties in classical abundance determination

Equivalent widths. Equivalent width measurements tend to have 3—5% uncertainty in the optical for a given measurement recipe (Gurtovenko & Kostik 1989); larger differences may result when different methods are used, as is the case for Oxford–Kiel comparisons discussed in Sect. 5.3 below.

Another source of difference is due to data quality. Most workers employ the Jungfraujoch atlas of Delbouille et al. (1973) taken with the double-pass grating spectrometer at the Jungfraujoch, but the segmented concatenation of the many discrete scans that make up this atlas represents a source of low-frequency modulation at the 3% level that affects continuum placement. A better tactic is to use wide-band scans from the Kitt Peak Fourier Transform Spectrometer, which also supplies higher spectral purity. Both points are demonstrated in Rutten (1988b).

To evaluate such uncertainties we have recomputed the 22 Kiel lines after increasing the Kiel W values by 3%; the effect on the fitted abundance A is shown in the top panel of Fig. 1. The corrections are small ($\Delta A \approx 0.01$ dex) for the weak lines at left and reach a maximum of $\Delta A \approx 0.05$ dex for $W \approx 10$ pm.

Partition functions. We employ the polynomial approximation of Irwin (1981) to compute partition functions for Fe I and Fe II. On average they are 6% larger than the values from Allen (1976) for the pertinent temperature range, whereas they are 12% smaller than the values given by Halenka & Grabowski (1984). Tests with the 22 Kiel lines show a 0.02 dex difference in resulting mean abundance for the Irwin–Allen difference, with an error of 0.01 dex when the temperature dependence is neglected. Changing Irwin's values by 12% produces a corresponding 0.05 dex change in A.

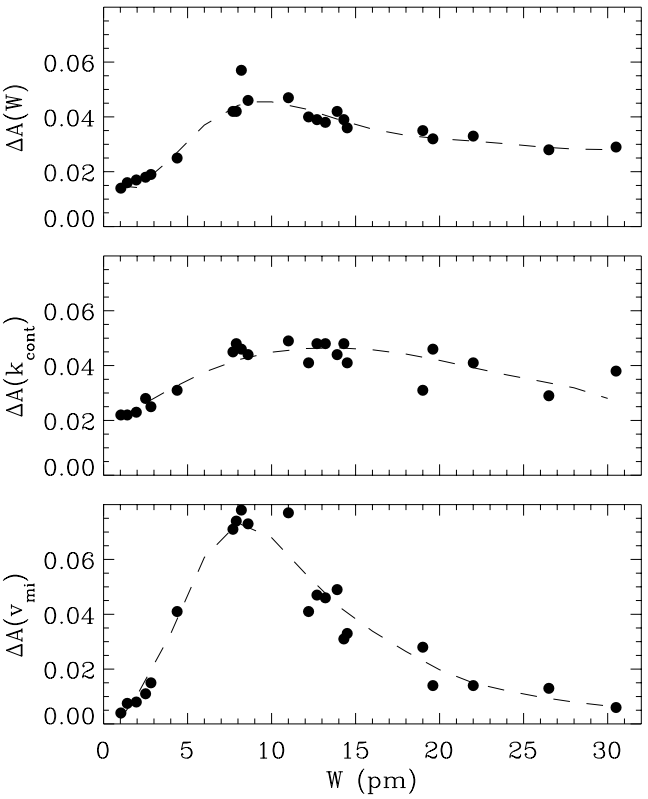

Fig. 1. Abundance changes ΔA against equivalent width W for the 22 Kiel lines and the Kiel parameters, respectively due to 3% increase of the observed equivalent width W (top), 10% change of the continuous opacity (middle), and 0.2 km s^{-1} change of the microturbulence $v_{\rm mi}$ (bottom)

Continuous opacity. The dominant source of continuous opacity in the visible region consists of photoionization of negative hydrogen H^-, contributing 90% while H^- free-free absorption adds 8–9% and bound-free transitions in metals and continuum scattering add less than 1%. The uncertainty of the bound-free cross-section of H^- is estimated to be 10% by Kurucz (1974). The largest uncertainty is due to the so-called "line haze" made up by unresolved weak lines and/or the overlapping wings of nearby strong lines, which may reach 10% in the violet (Holweger 1970, Vernazza et al. 1976, Rutten & van der Zalm 1984).

The middle panel of Fig. 1 displays abundance changes that result from a 10% change of the continuous opacity in our code. They are in the range 0.02–0.05 dex, in good agreement with the more elaborate correction curves in Fig. 2 of Rutten & van der Zalm (1984). The latter were derived from NLTE line formation modeling but also hold for classical LTE modeling using the Holweger-Müller model photosphere. They show, as does our test here, that using a high "true" continuum rather than the observed "local" continuum produces large errors in the equivalent width of weaker lines. An example is given by the large disparity for Fe I 524.70 nm in Table 5 below. The Ox-

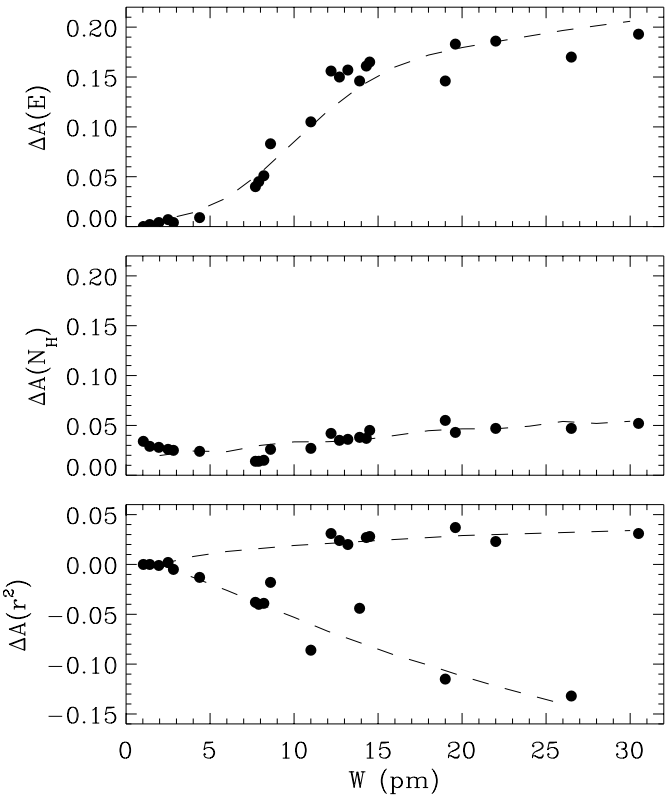

Fig. 2. Abundance changes ΔA against equivalent width W for the 22 Kiel lines and the Kiel parameters, due to difference in damping enhancement E (top), hydrogen density $N_{\rm H}$ (middle), and damping formalism (bottom)

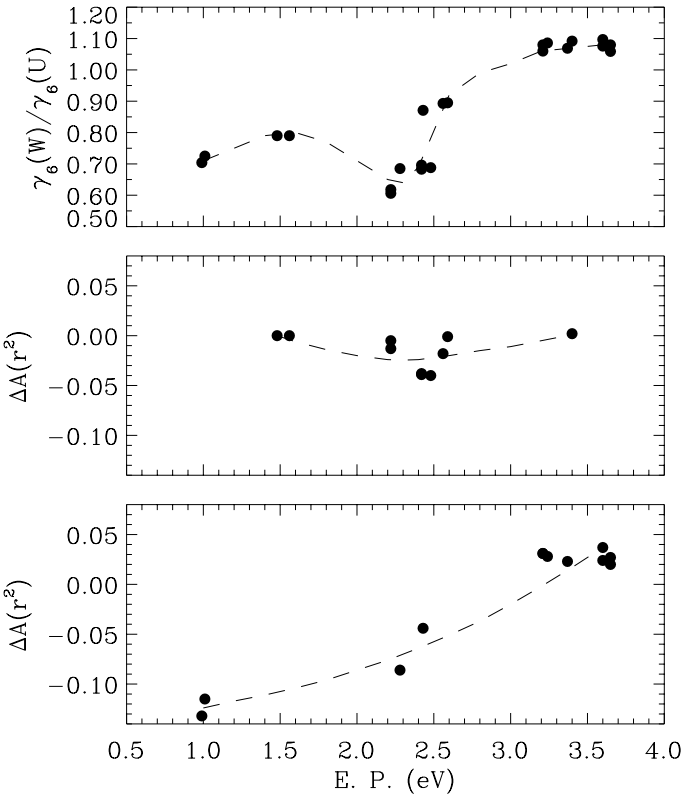

Fig. 3. The effect of van der Waals damping formalism against lower-level excitation energy, for the 22 Kiel lines. Top: ratio between van der Waals constants γ_6 obtained from the mean square radii of Warner (1969) and from the dipole approximation ignoring the azimuthal term in Eq. (3) and setting $\Delta_i = 0$ in Eq. (4). Middle: corresponding abundance errors for weak lines ($W < 10$ pm). Bottom: corresponding abundance errors for strong lines ($W \geq 10$ pm)

ford and Kiel W measurements for this line differ by more than 0.5 pm or 8%. We regain the Oxford value if we use the nominal 100% level of the Jungfraujoch atlas. Simply taking the local continuum without line-haze correction is a much better option. Using the correction curves of Rutten & van der Zalm (1984) is yet better; the best is to synthesize the background in detail.

Microturbulence. The microturbulence parameter $v_{\rm mi}$ serves in abundance studies to correct for the neglect of inhomogeneities. In their monograph Gurtovenko & Kostik (1989) conclude that $v_{\rm mi} \approx 0.8 - 1.0$ km s^{-1} across the formation heights of weak to strong Fe I lines. The bottom panel of Fig. 1 shows the change in A corresponding to this 0.2 km s^{-1} range; its size is similar to the results of Holweger et al. (1991). The lines of intermediate strength ($W \approx 6 - 12$ pm) are most sensitive to $v_{\rm mi}$. The 22-line average is $\Delta A(v_{\rm mi}) = 0.034$ dex.

Damping constant. The damping constant γ of Fe I lines is traditionally determined as the sum $\gamma = \gamma_{\rm rad} + \gamma_4 + \gamma_6$ of van der Waals broadening γ_6, quadratic Stark broadening γ_4 and radiative broadening $\gamma_{\rm rad}$. The main contribution is given by van der Waals broadening by H I and He I atoms and H_2 molecules; we test its influence here. According to the classical Weisskopf impact theory as improved by Lindholm (see Sect. 9-3 and Table 9-1 of Mihalas 1978):

$$\gamma_6 = 2\pi \sum_{k=1}^{3} \rho_k^2 \, N_k \, v_k , \qquad (1)$$

where $k = 1$, 2, 3 denotes the perturbers H I, He I and H_2, N_k the perturber density, v_k the mean relative velocity between the iron atom and the perturbing particle, and ρ_k the effective impact parameter given by $\rho_k = 1.648 (C_k / v_k)^{1/5}$ where the interaction constant is given by $C_k = 9.75\,10^{-10}\,\alpha_k\,\Delta r^2$, α_k is the perturber polarizability, and $\Delta r^2 = \overline{r}_{\rm u}^2 - \overline{r}_{\rm l}^2$ is the difference between the mean square radii of the upper level u and the lower level l of the transition. For neutral hydrogen as perturber the result is the classical equation (82,48) of Unsöld (1955):

$$\gamma_6 = 17.0 \; C_6^{2/5} \, v_{\rm H}^{3/5} \, N_{\rm H} , \qquad (2)$$

with $C_6 = 6.44 \times 10^{-34} \Delta r^2$ (82,54 in Unsöld 1955). Various laboratory measurements, theoretical predictions and empirical determinations have shown that γ_6 tends to exceed this estimate (see review by Kostik 1982); therefore, γ_6 is usually multiplied by a corrective enhancement factor E in the $E = 1 - 3$ range (cf. Gurtovenko & Kondrashova 1980, Gurtovenko & Kostik 1989). Thus, there are three error sources involved in setting γ_6, namely the enhancement factor E, the perturber densities N_k and the interaction constant C_6.

We first consider the enhancement factor E. The top panel of Fig. 2 shows the abundance effect of varying E between the Oxford value of $E = 1.2$ to the Kiel value of $E = 2.0$ for the 22 Kiel lines. The microturbulence was set to $v_{\rm mi} = 0.9\,{\rm km\,s^{-1}}$, being the average of the Kiel and Oxford values. The resulting change $\Delta A(E)$ increases rapidly with line strength and reaches considerable size already for $W \approx 15$ pm; it is much larger than the ΔA variations in Fig. 1.

As to the densities H I is the most important perturber species, the H_2 density being several orders of magnitude smaller while the He I contribution to the total density remains at the 10% level throughout the photosphere. The neutral hydrogen density $N_{\rm HI}$ is not specified by Holweger & Müller (1974) and therefore needs to be evaluated. One approach is to derive $N_{\rm HI}$ from the tabulated model through evaluating the total hydrogen density and then compute the hydrogen ionization balance. A second approach is to solve all ionization equilibria in detail for the tabulated electron pressure, temperature and chemical composition. The latter method is often used, but is rather sensitive to the input abundances of the electron donors which should not differ from the ones used by Holweger & Müller (1974); we therefore prefer model-consistent evaluation following the first approach. The results of a test with 10% difference in $N_{\rm HI}$, characteristic for different compositions, is shown in the middle panel of Fig. 2; the average over the 22 lines amounts to 0.034 dex abundance change.

We now turn to the interaction constant C_6. For many Fe I levels, mean square radii $\overline{r}^2$ have been tabulated on the basis of Thomas–Fermi–Dirac wave functions by Warner (1969). In many cases, these are superior to the Coulomb approximation of Bates & Damgaard (1949) given by

$$\overline{r}^2 \approx \frac{n_{\rm eff}^2}{2Z^2}\left[5n_{\rm eff}^2 + 1 - 3l\,(l+1)\right] \qquad (3)$$

with $n_{\rm eff}$ and l the effective and angular quantum numbers and the charge Z equal to unity for Fe I. However, the latter is still often used, and so is the dipole simplification ignoring the azimuthal term $1 - 3l\,(l+1)$ as given in Eq. (82,55) of Unsöld (1955):

$$\overline{r}^2 \approx 2.5\,\frac{n_{\rm eff}^4}{Z^2} = 2.5\left[\frac{13.5\;Z}{\chi(i,k^{\rm ion})}\right]^2 \qquad (4)$$

with $\chi(i,k^{\rm ion})$ the ionization energy from level i of the atom to its parent level k of the ion. The latter should not be taken equal to the energy difference to the Fe II ground state for many Fe I levels with excited parents, i.e., with ionization thresholds Δ_i eV above the Fe II ground state. This additional energy Δ_i should be added into $\chi(i,k^{\rm ion})$ when evaluating $n_{\rm eff}$ in the simple Coulomb or dipole approximations, but often is not (Rutten & Zwaan 1983). The Thomas–Fermi–Dirac mean square radii of Warner 1969 take excited parentage properly into account.

These various approximations are tested in Table 3. The fifth and sixth columns show differences in fitted abundance A obtained for the 22 Kiel lines and the Kiel parameters for two cases. In the first case (fifth column, labeled BD–W) the Bates-Damgaard approximation (BD) is tested against the square radii of Warner (1969) (W), with the azimuthal term taken into account in Eq. (3) and excited parentage taken into account into the evaluation of $n_{\rm eff}$. The corresponding abundance differences are small.

Much larger differences result for the second case (sixth column, labeled U–W). It specifies the differences obtained when the abundances derived from Unsöld's (U) dipole approximation (4) using the Fe II ground state are compared with the abundances derived from Warner's (W) mean square radii. Thus, this test checks the combined error of neglecting the azimuthal term and setting $\Delta_i = 0$. The errors range from $\Delta A = -0.132$ to $\Delta A = 0.037$ dex, with a 22-line average of -0.014 dex. They are also plotted in the bottom panel of Fig. 2 and the lower panels of Fig. 3; the top panel of the latter figure shows the corresponding corrections to γ_6. These corrections display a striking dip near E.P. = 2.2 eV but the split between weak and strong lines in the lower two panels indicates that this is not an intrinsic property which might explain the Oxford 2.2 eV anomaly, and it is indeed not present in similar plots using Oxford lines. We return to this dip in Sect. 5.2. The bottom panel of Fig. 2 has a forked appearance due to the different sensitivity to excitation energy shown in Fig. 3; the strongest low-excitation lines display the largest errors.

Table 4. Input data for 19 selected Oxford lines. The equivalent widths W are from Kiev, as are the corresponding abundances A (taking $E = 1.2$ and $v_{\rm mi} = 0.9\,{\rm km\,s^{-1}}$)

λ [nm]	source	E.P.	log gf	W	A
			Oxford	Kiev	Kiev
444.54	b	0.09	−5.44	3.65	7.599
519.87	d	2.22	−2.13	9.96	7.707
540.57	e	0.99	−1.84	25.1	7.641
543.45	e	1.01	−2.12	19.0	7.630
606.54	f	2.61	−1.53	12.0	7.613
608.27	b	2.22	−3.57	3.40	7.601
612.02	a	0.91	−5.97	0.47	7.671
613.66	c	2.45	−1.40	13.9	7.568
626.51	b	2.18	−2.55	8.59	7.626
628.06	b	0.86	−4.39	5.98	7.597
635.38	a	0.91	−6.48	0.15	7.656
649.49	c	2.39	−1.27	16.2	7.553
649.89	b	0.96	−4.70	4.35	7.653
662.50	a	1.01	−5.37	1.39	7.653
675.01	b	2.42	−2.62	7.53	7.653
832.70	c	2.20	−1.53	18.2	7.598
838.77	c	2.18	−1.49	20.0	7.655
851.40	c	2.20	−2.23	12.4	7.676
868.86	c	2.18	−1.21	27.9	7.724

a: Blackwell et al. (1986); b: Blackwell et al. (1984); c: Blackwell et al. (1982a); d: Blackwell et al. (1982c); e: Blackwell et al. (1979); f: Blackwell et al. (1982b).

5. The three discrepancies

The above tests indicate that Fe I abundance determinations suffer most from uncertainties in the damping enhancements E, followed by the equivalent widths W and, for lines around $W = 10$ pm, the microturbulence $v_{\rm mi}$. We now turn to the various discrepancies, using the Kiel and Oxford line lists to isolate the effects of these parameters in the resulting abundances.

5.1. The Kiev–Oxford discrepancy

Our Kiev emulation of the Oxford results for four lines in Sect. 2 are obtained with Warner's mean square radii while at Oxford the damping parameters are evaluated using the dipole approximation of Eq. (4), a habit that we suspected at

Table 5. Input data for the 25 Oxford lines of Blackwell et al. (1984) and results taking $v_{\rm mi} = 0.845$ km s^{-1}

λ [nm]	E.P.	W Oxford	A Oxford	A(dipole) $\Delta_i = 0$	ΔA $\Delta_i = 0$	ΔA $\Delta_i \neq 0$	A $E =$ E.P.	A $E = 1.2$	W RZ	A RZ	W Kiev	A Kiev
438.92	0.05	7.17	7.664	7.656	0.008	0.008	7.677	7.666	-	-	7.06	7.634
444.54	0.09	3.88	7.663	7.657	0.006	0.006	7.659	7.658	3.67	7.610	3.65	7.605
522.55	0.11	7.10	7.689	7.688	0.001	0.001	7.701	7.692	-	-	7.13	7.699
524.70	0.09	6.58	7.683	7.681	0.002	0.002	7.693	7.687	-	-	6.04	7.549
525.02	0.12	6.49	7.685	7.683	0.002	0.002	7.696	7.690	6.34	7.650	6.49	7.690
595.67	0.86	5.08	7.661	7.664	−0.003	−0.002	7.667	7.666	4.85	7.617	4.87	7.621
608.27	2.22	3.40	7.607	7.606	0.001	0.002	7.610	7.610	-	-	3.40	7.609
613.69	2.20	6.38	7.573	7.577	−0.004	−0.002	7.590	7.594	-	-	6.35	7.588
615.16	2.18	4.82	7.572	7.573	−0.001	0.002	7.579	7.581	4.84	7.585	4.86	7.589
617.33	2.22	6.74	7.600	7.605	−0.005	−0.002	7.620	7.625	7.37	7.765	6.93	7.665
620.03	2.62	7.56	7.677	7.679	−0.002	−0.013	7.693	7.717	7.29	7.662	7.33	7.671
621.92	2.20	9.15	7.626	7.628	−0.002	0.005	7.663	7.678	-	-	9.13	7.671
626.51	2.18	8.68	7.625	7.629	−0.004	0.002	7.655	7.666	8.49	7.627	8.59	7.647
628.06	0.86	6.24	7.659	7.660	−0.001	0.000	7.672	7.669	-	-	6.21	7.662
629.78	2.22	7.53	7.616	7.619	−0.003	0.000	7.640	7.645	-	-	7.64	7.670
632.26	2.59	7.92	7.703	7.710	−0.007	−0.019	7.725	7.752	7.73	7.708	7.79	7.720
648.18	2.28	6.42	7.663	7.665	−0.002	−0.007	7.672	7.672	6.29	7.646	6.39	7.667
649.89	0.96	4.43	7.672	7.670	0.002	0.002	7.675	7.674	4.18	7.623	4.35	7.659
659.38	2.43	8.64	7.687	7.692	−0.005	−0.018	7.712	7.722	8.85	7.764	8.98	7.790
660.91	2.56	6.55	7.639	7.640	−0.001	−0.008	7.649	7.665	-	-	6.35	7.624
675.01	2.42	7.58	7.655	7.658	−0.003	−0.003	7.691	7.691	7.44	7.658	7.53	7.680
694.52	2.42	8.38	7.658	7.660	−0.002	−0.002	7.700	7.700	-	-	8.44	7.712
697.88	2.48	8.01	7.655	7.658	−0.003	−0.003	7.694	7.694	7.72	7.632	8.18	7.729
791.28	0.86	4.87	7.692	7.692	0.000	0.000	7.698	7.697	-	-	4.70	7.665
807.51	0.92	3.47	7.685	7.685	0.000	0.000	7.686	7.686	-	-	3.25	7.642

Table 6. Results in Table 5 averaged over bins of excitation energy, plus bin-averaged results from Blackwell et al. (1995)

E.P.	Oxford	A(dipole)	$A(E =$ E.P.)	$A(E = 1.2)$	A(RZ)	A(Kiev)	A(Oxford95)
0.05–0.12	7.677±0.012	7.673±0.015	7.685±0.017	7.679±0.014	7.630±0.020	7.635±0.062	7.669±0.013
0.86–0.96	7.674±0.015	7.674±0.014	7.680±0.012	7.678±0.012	7.620±0.003	7.650±0.018	7.647±0.025
2.18–2.22	7.603±0.023	7.605±0.023	7.622±0.032	7.628±0.036	7.659±0.037	7.634±0.038	7.610±0.027
2.28–2.28	7.663	7.665	7.672	7.672	7.646	7.667	7.667±0.014
2.42–2.62	7.668±0.022	7.671±0.024	7.695±0.024	7.706±0.024	7.706±0.024	7.704±0.042	7.639±0.018
all lines	7.652±0.036	7.653±0.036	7.668±0.037	7.672±0.039	7.657±0.056	7.658±0.051	7.641±0.029
dip	−0.069	−0.067	−0.065	−0.061	+0.002	−0.034	−0.041
rms	±0.029	±0.029	±0.046	±0.043	±0.061	±0.066	±0.035

first and that eventually was confirmed by the manuscript of Blackwell et al. (1995). Figures 2–3 show sizable differences between these two evaluations of γ_6. The modeling of all 25 Fe I lines used by Blackwell et al. (1984) is therefore repeated in Table 5. The first three columns specify the lines and the Oxford input data. The fourth column (labeled A Oxford) gives the Oxford A values derived by Blackwell et al. (1984).

The next column (labeled A(dipole), $\Delta_i = 0$) contains the abundance values that we obtain with the Oxford input parameters (including excitation-dependent E) when using Eq. (4) neglecting parentage excitation. The differences with the Oxford values are given in the sixth column (ΔA, $\Delta_i = 0$). They are small; they range from −0.007 to 0.008 dex and the average absolute difference is only 0.003 dex. These results are averaged over bins in excitation energy in Table 6. The differences between the binned Oxford and dipole results in columns two and three are virtually zero.

The seventh column of Table 5 (labeled $\Delta_i \neq 0$) shows similar differences with the Oxford values obtained when Eq. (4) is used with proper parentage excitation. The differences remain small, showing that the Δ_i parentage corrections are not very important. Thus, our Kiev code reproduces the Oxford results closely when we employ the simple dipole estimate in Eq. (4) with or without parentage corrections.

Another damping difference lies in the dependence of E on excitation energy. This difference is also tested in Table 5, now using the mean square radii of Warner (1969). The eighth column (labeled $E =$ E.P.) has E increasing with excitation energy in Oxford manner (note that Kostik 1982 suggested that E should rather decrease with excitation energy), while the next column is for constant $E = 1.2$. The effect of this choice is also small, only 0.006 dex for the average of the absolute differences between these two columns.

Larger differences result from comparing column eight with

the Oxford results in the fourth column, effectively measuring the neglect of the azimuthal term in Eq. (3). The differences between the abundances in column eight (using Warner's square radii) and the Oxford results in column four range from −0.042 to 0.004 dex; their absolute average is 0.016 dex. Thus, the Oxford practice to employ the dipole approximation when evaluating van der Waals damping constants explains the Kiev–Oxford code discrepancy.

5.2. The 2.2 eV anomaly

Collisional damping. The top panel of Fig. 3 shows a sizable dip for lines with lower-level excitation potential near E.P. = 2.3 eV, indicating that the anomaly for 2.2 eV lines claimed by Blackwell et al. (1984) may also have to do with the evaluation of the mean square radii. We test this in Table 6 by combining the lines in Table 5 in bins of different excitation energy in Oxford manner. The third bin (2.18–2.22 eV) contains the 2.2 eV lines. The average over this bin is indeed on the small side for the Oxford results in the second column. The bottom two lines of Table 6 quantify this deficiency by specifying as "dip" the difference between the binned 2.18–2.22 eV abundances and the mean abundance for all other lines in Table 5, with the corresponding rms variation around this difference given in the last line. The dip indeed exceeds its 1 σ uncertainty for the Oxford results.

The fourth and fifth columns, again binning the abundance fits of the corresponding columns in Table 5, show that the dip becomes less significant when Warner's mean square radii are employed instead of the dipole approximation. It keeps its size but the rms uncertainty increases.

Equivalent widths. The top panel of Fig. 1 as well as the debates in Blackwell et al. (1995) and Holweger et al. (1995) indicate that the equivalent width W is the next sensitive parameter after the collisional damping. The remaining columns in Table 5 and the sixth and seventh columns of Table 6 therefore employ independent W's for the 25 Oxford lines. The equivalent widths marked W(RZ) are taken from the clean-line list of Rutten & van der Zalm (1984) for the lines of overlap, while the column W(Kiev) specifies values determined by Gurtovenko & Kostik (1989). These were used to fit the iron abundance using $E = 1.2$, $v_{\rm mi} = 0.845\,{\rm km\ s^{-1}}$ (the Oxford value) and Warner's square radii; the results are given in the columns A(RZ) and A(Kiev). The mean difference between the Oxford and Kiev W's is only 2.2%; the mean W difference Oxford–RZ is 3.5%. These small differences cause appreciable decrease of the dip, however; it vanishes for the clean-line RZ values and is within the rms uncertainty for the Kiev values. Thus, the combined effect of uncertainties in equivalent width measurements and differences in γ_6 evaluation is to make the 2.2 eV anomaly statistically insignificant.

New data from Oxford. Finally, the last column of Table 6 specifies similar bin averages for the new Oxford results of Blackwell et al. (1995), in which some new lines were added, some old lines were replaced by new ones, and new W measurements were used also for the old lines. The dip is smaller and less significant in these new Oxford results also.

Table 7. Equivalent widths and corresponding abundances for the 22 Kiel lines of Table 3 ($E = 2.0$, $v_{\rm mi} = 1.0\,{\rm km\ s^{-1}}$)

λ [nm]	W Kiel	W Kiev	W Oxf.	A Kiel	A Kiev	A Oxf.
521.73	12.2	12.4	13.14	7.52	7.55	7.63
532.41	30.5	31.8	33.50	7.54	7.60	7.64
539.31	14.5	16.0	17.70	7.38	7.52	7.63
540.57	26.5	25.9	26.90	7.52	7.53	7.57
543.45	19.0	18.7	20.90	7.41	7.40	7.53
558.67	22.0[1]	26.0	29.80	7.31	7.51	7.64
570.15	8.60	8.57	8.95	7.49	7.50	7.56
577.84	1.95	2.01	2.05	7.48	7.50	7.52
578.46	2.50	2.43	2.55	7.48	7.47	7.50
608.27	2.82	3.40	3.35	7.48	7.60	7.59
624.06	4.38	4.83	4.83	7.43	7.51	7.51
624.63	12.7	12.4	14.20	7.44	7.42	7.60
630.15	13.2	13.7	14.40	7.52	7.58	7.64
639.36	13.9	14.2	15.05	7.35	7.39	7.47
640.00	19.6	19.6	22.50	7.49	7.51	7.66
641.16	14.3	14.3	16.15	7.49	7.50	7.64
642.13	11.0	10.8	11.40	7.43	7.40	7.49
658.12	1.41	1.67	1.67	7.43	7.52	7.52
673.95	1.03	1.11	1.10	7.45	7.49	7.49
675.01	7.70	7.52	7.70	7.60	7.56	7.60
694.52	8.20	8.45	8.40	7.50	7.55	7.54
697.88	7.90	8.18	8.10	7.54	7.59	7.58
$\overline{A}$				7.47	7.51	7.57
rms				±0.07	±0.06	±0.06

[1] The Kiel value $W = 22.0$ pm for this line is too low, through oversight of the correction to $W = 25.5$ pm given by Garz et al. (1970) (see Holweger et al. 1995)

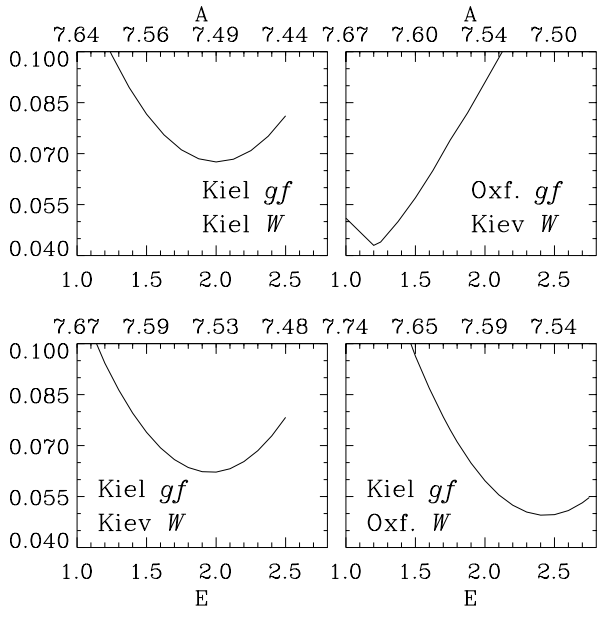

Fig. 4. Dependence of rms variation ε in mean fitted abundance on damping enhancement factor E. The corresponding abundance values are indicated along the top of each panel. Upper left: 22 Kiel lines, Kiel gf and W values. Upper right: 19 Oxford lines, Oxford gf values, W's from Kiev. Lower left: 22 Kiel lines, Kiel gf values, W's from Kiev. Lower right: 22 Kiel lines, Kiel gf values, W's from Oxford. The minima define the "neck" or "best choice" of E

5.3. The Kiel–Oxford discrepancy

The tests in Sect. 4 and the results above indicate that we should concentrate on the equivalent width W and the damping enhancement factor E as the parameters that may lie at the heart of the Kiel–Oxford discrepancy. They are also debated by Blackwell et al. (1995) and Holweger et al. (1995). In addition, there is an average offset between the Hannover and Oxford *gf* scales, and there may be effects from difference in line selection.

Equivalent widths. In their 1995 analysis, the Oxford group re-measures and discusses the W values of the 22 Kiel lines. We do the same here. Table 7 specifies the original W values from Holweger et al. (1991) (second column) together with our own measurements (third column) and those of the Oxford group (fourth column). The W measurements of Blackwell et al. (1995) exceed those of Holweger et al. (1991) in all cases except Fe I 675.01 nm, often considerably. The averaged Oxford–Kiel W differences are 7% for the weak lines ($W < 5$ pm), 3% for the intermediate lines ($5 < W < 10$ pm) and 13% for the strong lines ($W > 10$ pm). In contrast, our Kiev W determinations are closer to the Kiel values, with differences of either sign.

Holweger et al. (1995) attribute the systematic Oxford excesses for the strongest lines to the difference between the Kiel practice of cutting extended wings in both observation and modeling and the Oxford practice of including them far out. (At Kiev, the profiles are cut at line depression $d = 0.0005D$ with D the central depression.) For the other lines, Holweger et al. (1995) attribute the Oxford excesses to too high continuum placement (see Sect. 4 above).

The remaining columns of Table 7 give corresponding iron abundance values. The fifth column (labeled A Kiel) specifies the original results of Holweger et al. (1991), the next column (A Kiev) gives the abundance values that we obtain from our own measurements (W Kiev) using the Kiel input parameters ($E = 2$, $v_{\rm mi} = 1.0$ km s^{-1}) and Warner's square radii, and the last column (A Oxford) contains the abundances that are obtained by us from the Oxford W values again using the Kiel input parameters and Warner's square radii. The Oxford–Kiel abundance differences are sizable, 0.10 dex for the all-line average, 0.05 dex for the weak and intermediate line average and 0.145 dex for the strong-line average. Therefore, an appreciable part of the Kiel–Oxford discrepancy may originate from W differences.

Collisional damping. We now turn to the damping enhancement factor E. We have used our Kiev code to determine abundance values A for the 22 Kiel lines of Table 3 with the Kiel *gf* and W values, and also for the comparable selection of 19 Oxford lines of Table 4 using the Oxford *gf* values with the Kiev W's listed in Table 4. We used our own measurements in this case because there are only a few W values available from Oxford for these lines. The microturbulence was set to the Oxford–Kiel average $v_{\rm mi} = 0.9$ km s^{-1} and the mean square radii were again taken from Warner (1969). The damping enhancement factor E was taken constant with excitation energy; its value was varied to obtain a range of corresponding abundance values per line. Our results for the 19 Oxford lines using $E = 1.2$ are specified in the last column of Table 4.

The results were averaged per value of E over the lines in each set; the corresponding rms variations ε in fitted abundance are plotted against E in Fig. 4. The corresponding averaged abundance is specified (on a non-linear scale) along the top of each panel, larger E producing smaller A. The minima of these curves show, according to the "neck" modus of abundance determination, the preferable combination of E and A for the given set of lines and input data. These are, respectively, $E = 1.9$ and $A = 7.50 \pm 0.07$ for the 22 Kiel lines (upper-left panel) and $E = 1.2$ and $A = 7.64 \pm 0.04$ for the 19 Oxford lines (upper-right panel). These minima agree with the E values actually used at Kiel and Oxford.

Comparison of the upper panels in Fig. 4 at a given E value produces smaller difference in A when the offset of 0.034 dex between the two *gf* scales is also taken into account. Such comparison for $E = 1.0$ shows that the mean difference A(Oxford) $-$ A(Kiel) $= 7.67 - 7.64 + 0.034 = 0.00$ while at $E = 2.5$ it is A(Oxford) $-$ A(Kiel) $= 7.50 - 7.44 + 0.034 = 0.03$.

The striking difference in best choice of E between the two upper panels may have to do with the systematic difference between the Kiel and Oxford W determinations diagnosed above. We have therefore repeated the analysis of the Kiel lines using our own W's (lower-left panel) and the Oxford W's of the same lines given by Blackwell et al. (1995) (lower-right panel). The small difference between the Kiel and Kiev W measurements results in small difference between the two lefthand panels, but the lower-right panel shows a large shift of the curve towards higher E. The A scale along the top is also shifted. Thus, the average excess of the Oxford W values over the Kiel and Kiev measurements is divided between increase of E and increase of A in such an analysis. The minimum in the lower-left panel is at $E = 1.9$ and $A = 7.53 \pm 0.06$, to be compared with $E = 1.9$ and $A = 7.47$ of Holweger et al. (1991), which is their result before correction for NLTE ionization. In the lower-right panel the minimum is at $E = 2.4$ and $A = 7.54 \pm 0.05$. These abundance values differ less than one might expect from the curve differences because the curve shift and the A shift relative to E have opposite sign.

Oscillator strengths. Comparison of the upper-right and lower-left panels of Fig. 4 represents a relatively direct comparison of the Oxford and Hannover *gf* values because the input parameters are the same, E is varied similarly for both, and the equivalent widths W are from us in each case, i.e., determined the same way without introducing systematic differences. The two minima produce abundance values $A = 7.64$ and $A = 7.53$, respectively. Their difference exceeds the difference resulting from the upper-left lower-right comparison for W effects; this indicates that *gf* differences play a role as well.

In order to search for *gf* effects affecting Kiel–Oxford comparisons, it is better to make distinction between lines of different strength rather than average all lines without discrimination in obtaining "best fits" as in Fig. 4, and to look at the actual variation of the spread along line strength. We do this in Fig. 5, maintaining some variation in E by plotting separate panels for $E = 1.2$ (the Oxford choice) and $E = 1.9$ (the Kiel choice). The upper half of Fig. 5 is for abundance fits A_W of the equivalents widths W measured at Kiev, using the Hannover *gf* values for the 22 Kiel lines at left and the Oxford *gf* values for the 19 Oxford lines at right. The solid curves are fits to all lines. The dashed fits in the lefthand panels hold for a subset of the Kiel lines excluding two categories not present in the Oxford

sample. The first is formed by the seven lines marked by stars; they have $\log gf > -1.0$. The second group consists of deeply-formed lines with line-center formation height $h_D < 200$ km. Both categories are discussed in Section 6.

The differences between the lefthand Kiel and righthand Oxford panels are striking. In both cases, larger E reduces A considerably for the stronger damping-sensitive lines, but the Kiel curves show upward trends with W while the Oxford curve in the lower-right A_W panel slopes down. For each, the slope of the fitted curves is smallest at the E value where the corresponding minimum in Fig. 4 occurs. Therefore, these rms minima measure the absence of such slopes, rather than the amount of random scatter around a mean value. The presence of systematic trends must be explained rather than averaged away in rms curves.

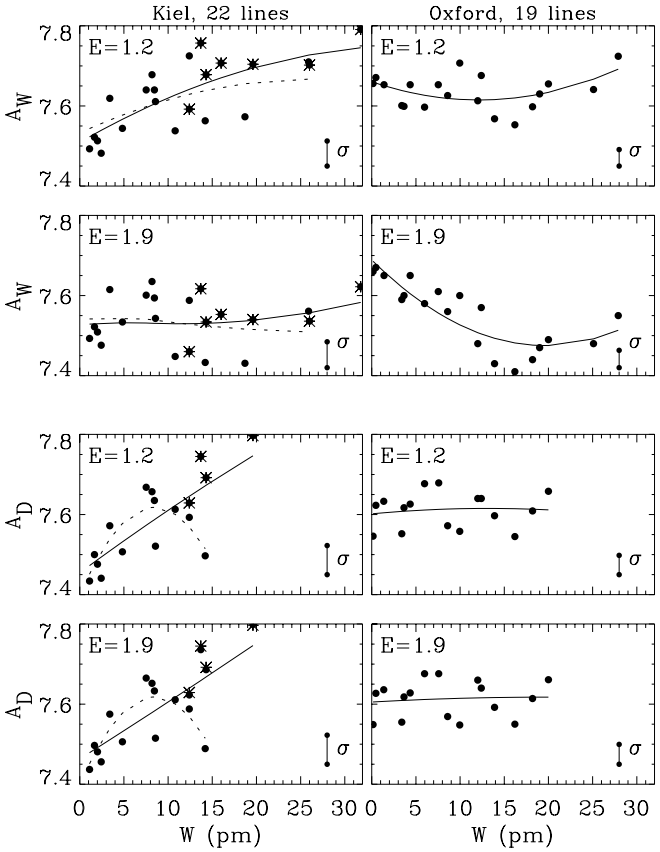

Fig. 5. Iron abundances A_W determined from equivalent widths and A_D determined from line depths against observed equivalent width W. Left: the Kiel lines of Table 3. The A_D panels contain only 17 lines because lines with depth $D > 0.8$ are excluded. Right: the Oxford lines of Table 4. The A_D panels contain 16 lines. The solid curves are least-square second-order polynomial fits. The stars in the Kiel panels mark lines with $\log gf > -1$. They are excluded in the dotted fits, as are all lines with formation height $h_D < 200$ km. The bars marked σ specify the standard deviation of the solid fits

Line depth fits. The above tests and comparisons show that the A_W and E determinations interfere strongly. Since abundance fits are actually fits of the product gfA, this cross-talk exists also between E and the input gf values. For example, if the gf values produce an erroneous trend with W in the fitted abundances, it may easily be canceled by empirical adjustment of E to make the stronger lines yield the same abundance as the weaker lines. In order to reduce this awkward sensitivity to the E parameter we have fitted abundances A_D for the 22 Kiel lines and 19 Oxford lines to the observed central line depths $D = (I_{\rm cont} - I_{\rm line})/I_{\rm cont}$. These A_D fits are sensitive to the macroturbulence $v_{\rm ma}$ and also have larger sensitivity to departures from LTE than A_W fits, but their sensitivity to E is much smaller. Gurtovenko & Kostik (1989) have shown that errors in A_D from D uncertainties remain small as long as the central line depths do not exceed $D = 0.8$. Deeper lines suffer from saturation.

We measured the central depths of the Kiel and Oxford lines from the Jungfraujoch Atlas following Gurtovenko & Kostik (1989), discarding all lines with $D > 0.8$. The macroturbulence $v_{\rm ma}$ was chosen to give the smallest spread in fitted abundances A_D for the nine lines of overlap marked in Tables 8 and 9. The gf differences between these are small. The resulting values are $v_{\rm ma} = 1.62$ km s^{-1} and 1.55 km s^{-1} for the Kiel and Oxford lines, respectively, in good agreement with the value $v_{\rm ma} = 1.63$ km s^{-1} of Holweger et al. (1978). We have used the mean value $v_{\rm ma} = 1.6$ km s^{-1}. The precise value is not very important as shown by Gurtovenko & Kostik (1989) and Gurtovenko & Sheminova (1988); a change of 0.1 km s^{-1} produces only 0.03–0.04 dex change in A_D.

The results are shown in the lower half of Fig. 5. The reduced dependence on E in these D fits is obvious since the upper and lower panels are about equal for both the Kiel and the Oxford lines. The Oxford gf values now produce virtually flat fits at $A_D \approx 7.6$ in both cases, whereas the Kiel gf values produce a suspicious-looking steep increase from $A_D = 7.48$ for weak lines to $A_D = 7.75$ near $W = 20$ pm.

Comparison of the A_D panels with the A_W panels indicates that $E = 1.2$ is the better choice. The corresponding A_W panels show behavior that is similar to the A_D panels for both the Kiel and the Oxford lines, whereas the $E = 1.9$ panels with A_W fits depart from the A_D patterns. The A_D panels then confirm that the Oxford lines produce abundance values that roughly obey the classical assumption of quasi-random scatter around a mean value, for which the rms variation may be taken as precision indicator. In contrast, the Kiel lines produce abundance values that have a steep systematic trend with line strength. This trend difference represents the greater part of the Kiel–Oxford discrepancy.

Fig. 6 compares the upper and lower halves of Fig. 5 explicitly by plotting the differences $A_W - A_D$ in the two fits per line, both for $E = 1.2$ (solid) and $E = 1.9$ (dashed). The $E = 1.2$ curves are close to $A_W - A_D = 0$ in both the Kiel and the Oxford panels, whereas the $E = 1.9$ curves drop to $A_W - A_D \approx -0.2$ near $W = 20$ pm. The comparison again indicates that $E = 1.2$ is the better choice.

In conclusion, our comparisons of the 22 Kiel lines and the 19 Oxford lines show that the Kiel-Oxford discrepancy stems from systematic differences in equivalent widths W and in oscillator strengths gf that affect the choice of the damping enhancement E. The two effects are separated in Fig. 4 (in which the three Kiel gf panels compare results for three sets of W measurements) and in Fig. 5 (for which we used our own W's for both sides). The significant trend difference in the latter figure requires further scrutiny.

Table 8. Input data for 36 Oxford lines and abundances A_D obtained from line depths D ($E = 1.5$, $v_{\rm mi} = 0.9\,{\rm km\ s^{-1}}$, $v_{\rm ma} = 1.6\,{\rm km\ s^{-1}}$)

λ [nm]	E.P.	log gf Oxf.	W Oxf.	D Kiev	A_D Kiev
444.54	0.09	−5.44	3.88	0.573	7.618
519.87	2.22	−2.13	9.96[2]	0.792	7.545
524.70	0.09	−4.95	6.58	0.716	7.609
525.02	0.12	−4.94	6.49	0.710	7.605
570.15[1]	2.56	−2.23	8.51	0.711	7.609
595.67	0.86	−4.60	5.08	0.538	7.617
606.54	2.61	−1.53	11.9[2]	0.754	7.661
608.27[1]	2.22	−3.57	3.40	0.363	7.553
612.02	0.91	−5.97	0.47[2]	0.052	7.625
613.66	2.45	−1.40	13.9[2]	0.768	7.583
613.69	2.20	−2.95	6.38	0.611	7.580
615.16[1]	2.18	−3.30	4.82	0.507	7.577
617.33	2.22	−2.88	6.74	0.622	7.587
620.03	2.61	−2.44	7.56	0.631	7.601
621.92[1]	2.20	−2.43	9.15	0.697	7.609
625.25	2.40	−1.69	12.3[2]	0.741	7.563
626.51	2.18	−2.55	8.68	0.678	7.568
628.06	0.86	−4.39	6.24	0.612	7.676
629.78[1]	2.22	−2.74	7.53	0.649	7.628
632.26	2.59	−2.43	7.92	0.634	7.627
635.38	0.91	−6.48	0.15[2]	0.014	7.548
643.08	2.18	−2.01	11.05[2]	0.725	7.584
648.18[1]	2.28	−2.98	6.42	0.573	7.616
649.49	2.39	−1.27	16.2[2]	0.753	7.552
649.89	0.96	−4.70	4.35	0.442	7.628
657.42	0.99	−5.00	2.65	0.293	7.633
659.38	2.43	−2.42	8.64	0.646	7.621
660.91	2.56	−2.69	6.55	0.563	7.595
662.50	1.01	−5.34	1.36	0.149	7.604
675.01[1]	2.42	−2.62	7.58	0.617	7.667
694.52[1]	2.42	−2.48	8.38	0.627	7.670
697.88[1]	2.48	−2.50	8.01	0.613	7.671
772.32	2.28	−3.62	3.85	0.336	7.675
832.70	2.20	−1.53	18.2[2]	0.676	7.615
838.77	2.18	−1.49	20.0[2]	0.682	7.661
851.40	2.20	−2.23	12.4[2]	0.613	7.640

[1] Lines of overlap with Table 9
[2] Equivalent width determined at Kiev

Table 9. Input data for 41 Kiel lines and abundances A_D obtained from line depths D ($E = 1.5$, $v_{\rm mi} = 0.9\,{\rm km\ s^{-1}}$, $v_{\rm ma} = 1.6\,{\rm km\ s^{-1}}$)

λ [nm]	E.P.	log gf Kiel	W Kiel	D Kiev	A_D Kiev
504.42	2.85	−2.06	7.50	0.722	7.515
521.73	3.21	−1.07	12.2	0.793	7.581
525.34	3.28	−1.57	8.10	0.725	7.578
532.99	4.08	−1.19	5.60	0.598	7.479
541.28	4.43	−1.72	1.78	0.205	7.434
549.18	4.19	−2.19	1.06	0.130	7.437
552.55	4.23	−1.08	5.80	0.550	7.413
566.13	4.28	−1.76	1.98	0.233	7.416
570.15[1]	2.56	−2.13	8.60	0.711	7.519
570.54	4.30	−1.36	3.90	0.398	7.416
577.84	2.59	−3.44	1.95	0.233	7.478
578.46	3.40	−2.53	2.50	0.275	7.451
585.51	4.61	−1.48	2.10	0.223	7.436
608.27[1]	2.22	−3.59	2.82	0.363	7.573
615.16[1]	2.18	−3.27	4.56	0.507	7.547
621.92[1]	2.20	−2.42	8.70	0.697	7.588
624.06	2.22	−3.23	4.38	0.488	7.508
624.63	3.60	−0.73	12.7	0.716	7.628
627.12	3.33	−2.70	2.09	0.229	7.460
629.78[1]	2.22	−2.73	7.30	0.649	7.613
630.15	3.65	−0.72	13.2	0.719	7.743
633.68	3.69	−0.86	11.6	0.698	7.711
639.36	2.43	−1.43	13.9	0.745	7.485
640.00	3.60	−0.29	19.6	0.752	7.794
641.16	3.65	−0.60	14.3	0.717	7.689
642.13	2.28	−1.94	11.0	0.724	7.595
648.18[1]	2.28	−2.96	6.30	0.573	7.593
658.12	1.48	−4.68	1.41	0.178	7.502
666.77	4.58	−2.11	0.89	0.081	7.529
669.91	4.59	−2.10	0.73	0.071	7.466
673.95	1.56	−4.79	1.03	0.108	7.435
675.01[1]	2.42	−2.61	7.70	0.617	7.667
679.32	4.08	−2.33	1.10	0.116	7.452
680.42	4.58	−1.81	1.40	0.130	7.470
683.70	4.59	−1.69	1.54	0.159	7.469
685.48	4.59	−1.93	1.00	0.113	7.529
694.52[1]	2.42	−2.44	8.20	0.627	7.632
697.19	3.02	−3.34	1.20	0.113	7.426
697.88[1]	2.48	−2.48	7.90	0.613	7.654
718.91	3.07	−2.77	3.80	0.334	7.577
740.16	4.19	−1.60	4.10	0.349	7.555

[1] Lines of overlap with Table 8

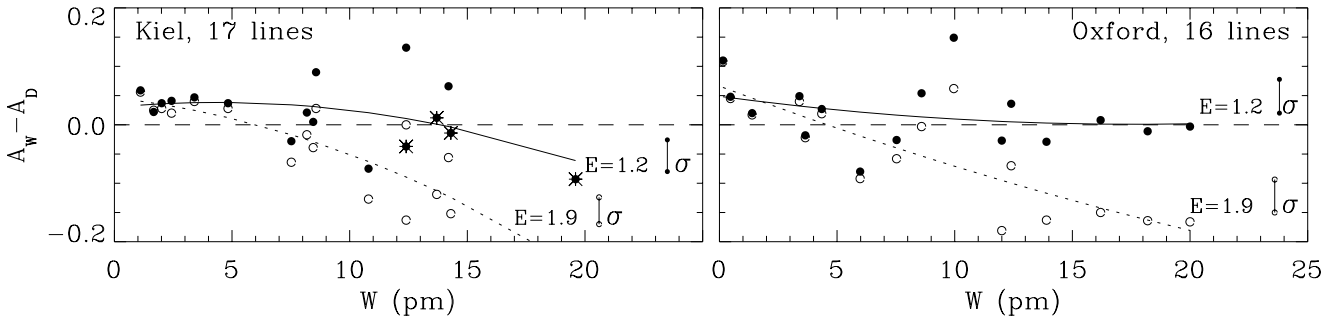

Fig. 6. Differences between line width and line depth abundance fits $A_W - A_D$ per line, against the observed equivalent width W. Left: Kiel lines from Table 3 with $D < 0.8$. Right: Oxford lines from Table 4 with $D < 0.8$. Solid dots, stars and solid fits: $E = 1.2$. The stars mark lines with $\log gf > -1$. Open circles and dashed fits: $E = 1.9$. The curves are least-square second-order polynomial fits with rms variations indicated by the 1σ bars

More line depth fits. Figure 5 demonstrates the usefulness of adding abundance determinations from line depths to the debate on abundances from equivalent widths. Our receipt of the manuscripts of Blackwell et al. (1995) and Holweger et al. (1995) has enabled us to expand such A_D analysis to larger samples of Oxford and Kiel lines. They are specified in Tables 8 and 9. There are nine lines of overlap between the two sets that are marked in both tables.

The 36 Oxford lines come from Table 6 of Blackwell et al. (1995) (25 lines), our Table 4 (8 lines), Blackwell et al. (1982b) (606.549 nm) and Blackwell et al. (1982a) (625.256 nm and 643.085 nm); the 41 Kiel lines are from Holweger et al. (1991, 1994). All lines have $D < 0.8$; the selection of Oxford lines aims to give similar W coverage as for the Kiel lines. Their depths D were again measured from the Jungfraujoch Atlas and are given in Tables 8 and 9, together with the iron abundance values A_D that we obtain from them setting $E = 1.5$, $v_{\rm mi} = 0.9\,{\rm km\ s^{-1}}$ and $v_{\rm ma} = 1.6\,{\rm km\ s^{-1}}$. We emphasize again that the advantage of fitting line depths is the reduced sensitivity to the collisional-damping enhancement factor E. Figure 5 shows that taking the mean value $E = 1.5$ is a good choice that won't influence the results. The equivalent widths W in Tables 8–9 are from the Oxford and Kiel papers, except for a few Oxford lines marked in Table 8 for which we measured W values ourselves.

The top panels of Fig. 7 show the results in the same format as the lower panels of Fig. 5. The sample is larger but the result remains the same: the Oxford lines in the righthand panel scatter around a mean value $A_D = 7.62$ without noticeable systematic trends, whereas the Kiel lines in the upper-left panel produce a suspicious-looking increase with line strength that has appreciable magnitude. This difference pinpoints the Kiel–Oxford *gf* discrepancy.

6. Discussion

The top panels of Fig. 7 indicate that there is a problem with the Hannover *gf* values in Table 9. They produce the same steep trend that is seen in three of the four Kiel panels of Fig. 5. Such a trend is absent in the comparable Oxford panels; thus, the Kiel–Oxford discrepancy is transformed into a trend discrepancy. Since the other input parameters, the W measurement method, the code and all formalisms are the same for both sets, the obvious conclusion is that the Hannover *gf* values seem less reliable than the Oxford ones.

However, care is required before we blame the trend in the Kiel panel on the Hannover *gf* values. First, the trend contrast is actually reversed in the second panels of Fig. 5 for $E = 1.9$. Second, although the two sets have similar W coverage in the top panels of Fig. 7, they may differ in other ways that may cause selection effects. We discuss these issues in this section.

Yet more line fits. Plots as Fig. 6 in which the differences between fits of line widths and fits of line depths are plotted against line formation parameters have been made for many more lines in a Kiev tradition to derive empirical oscillator strengths from the solar spectrum. The same line synthesis techniques were used as employed in the classical abundance determination discussed here. Results, details and interpretations are given in the papers by Gurtovenko & Kostik (1981, 1982), Rutten & Kostik (1982, 1988), Rutten & Zwaan (1983), Rutten & van der Zalm (1984), Gurtovenko et al. (1990) and the monograph of Gurtovenko & Kostik (1989). We display results from the latter publication here, respectively for 731 Fe I lines in Fig. 8 and 62 Fe II lines in Fig. 9. Gurtovenko and Kostik fitted oscillator strengths gf_W from line widths and gf_D from line depths for a given iron abundance, but since *gf* values and abundance values enter the line extinction coefficient as the product gfA we may plot their results $\log gf_W - \log gf_D$ also as $A_W - A_D$ here. This is done in Figs. 8–9.

The 731-line display in Fig. 8 shows that fitting line widths and line depths in classical manner, assuming LTE, the Holweger-Müller model, a low value of E (in this case $E = 1.3$) and standard micro- and macroturbulence (close to the values $v_{\rm mi} = 0.9\,{\rm km\ s^{-1}}$ and $v_{\rm ma} = 1.6\,{\rm km\ s^{-1}}$ used for Figs. 5 and 6) produces excellent correspondence between the two approaches for nearly all suitable Fe I lines in the visible solar spectrum. The scatter remains below ± 0.1 dex for most lines; the rms spread around the fit in the top panel is only 0.05 dex. Moreover, the good correspondence holds for widely different excitation energies (lower panels). Thus, Fig. 8 shows that the assumptions of classical abundance determination produce excellent self-consistency between these two line measures. It doesn't prove the validity of the assumptions, but it does indicate that classical fitting as done here reaches a numerical

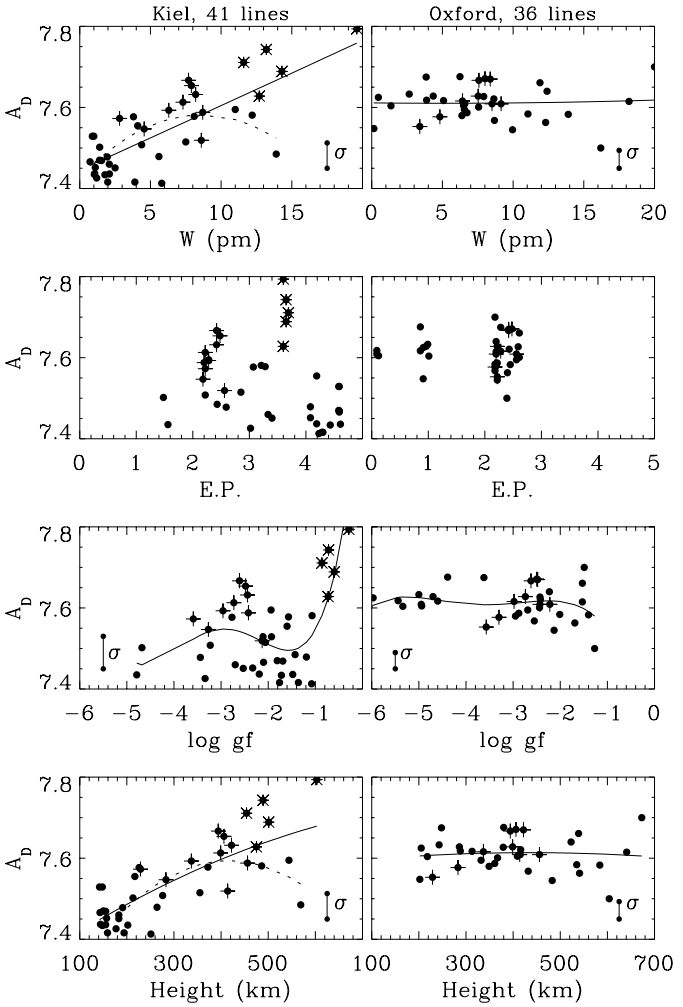

Fig. 7. Iron abundances A_D determined from the central depths D of Fe I lines, plotted from top to bottom against their observed equivalent widths W, their lower excitation potential E.P., the logarithm of their oscillator strength gf and the line-center height of formation h_D per line. Left: Kiel lines from Table 9. Right: Oxford lines from Table 8. The solid curves are least-square second-order polynomial fits; their rms variation is marked by the 1σ bars. The dotted curves in the top and bottom Kiel panels are similar second-order fits excluding all lines with $h_D < 200$ km and all lines with $\log gf > -1$; the latter lines are marked by stars. The crosses in both the Kiel and Oxford panels mark the nine lines of overlap between the two sets

precision of 0.1 dex or better. The 0.3 dex trend variations in Fig. 5 are therefore significantly large and worrisome.

In addition, Fig. 8 confirms that choosing $E = 1.2$ is preferable over setting $E = 1.9$. As indicated by Fig. 6, a large value of E makes the $A_W - A_D$ fit slope downward with height. That would require explanations from outside the assumptions of classical abundance determination, such as dropping LTE. We discuss these below; here, it suffices to note that adhering to the classical constraints makes $E = 1.2$ the better choice again.

Selection differences. Basically, solar Fe I lines differ in transition probability and in excitation energy; to first order, these properties determine their opacity and so set the solar line strength, height of formation, and sensitivity to collisional damping. The same properties set differences in the laboratory conditions needed for their measurement. In addition, differential effects may result from solar departures from LTE (affecting individual line opacities and/or line source functions) and from solar inhomogeneities (differentially felt through difference in response functions). The other panels of Fig. 7 therefore display our A_D fits again, but plotted against the basic transition properties. They serve to search for selection effects.

The second panels from above illustrate that the Oxford set does not contain any lines with E.P. ≥ 3 eV. Most lines cluster in a narrow E.P. range between 2 and 3 eV. In contrast, the Kiel set at left has no lines below E.P. < 1.4 eV. The Kiel lines with E.P. > 4 eV produce only small A_D values, whereas the Kiel lines with E.P. $= 2 - 3$ eV do not differ significantly in their A_D results from the 2–3 eV Oxford lines at right. The highest A_D values (stars) come from lines with E.P. ≈ 3.6 eV.

The third panels from above show that also the coverage of $\log gf$ differs between the Kiel and Oxford sets. There are five Kiel lines with $\log gf > -1$, whereas the Oxford set has none. These five lines are marked with stars in all Kiel panels of this figure. Four of them (Fe I 624.63 nm, 630.15 nm, 640.00 nm and 641.16 nm) are also present in the 22-line Kiel set and are also marked by stars in Fig. 5, together with three more lines with $\log gf > -1$. The five large-gf lines in the third Kiel panel of Fig. 7 produce strikingly large A_D values, whereas the lines with smaller transition probability do not show a systematic A_D pattern.

The bottom panels show the A_D fits against the height of line-center formation h_D. It is primarily set by the gf value and the excitation energy, with secondary sensitivity to the wavelength, the damping and to NLTE effects when present. The trends are the same as in the top panels, but this display shows that the low–A_D Kiel lines cluster below $h_D \approx 240$ km whereas the Oxford set does not contain any lines with $h_D < 200$ km. The large-gf lines in the Kiel set marked by stars are formed high in the atmosphere.

Lines of overlap. The main selection differences between the Kiel and Oxford panels in Fig. 7 are the absence of Oxford lines with $\log gf > -1$ (stars in Kiel panels), the absence of Oxford lines formed below $h_D = 200$ km, the absence of Oxford lines with E.P. > 3 eV and the absence of Kiel lines with E.P. < 1.4 eV. These selection differences are not independent; for example, there is only one Kiel line with $h_D < 200$ km and E.P. < 3 eV (Fe I 577.84 nm).

Most lines that correspond within these selection criteria are part of the cluster with E.P. $= 2 - 3$ eV in the second Oxford panel. Their behavior is well represented by the nine lines of overlap between the Kiel and Oxford sets, which are all within this E.P. bin. They are marked in Tables 9 and 8 and have been plotted with crosses in all panels of Fig. 7. Their A_D values are quite similar between the Kiel and Oxford sets, giving averages $A_D = 7.598$ for Kiel and $A_D = 7.622$ for Oxford. The small difference corresponds to their averaged oscillator strength difference $\Delta \log gf \approx 0.025$ dex between Oxford and Kiev.

Selection effects. The dotted fits in the top and bottom Kiel panels of Fig. 7 were obtained by excluding the five lines with $\log gf > -1$ marked by stars and also all lines with $h_D < 200$ km. The five large-gf lines set the upper end of the trend

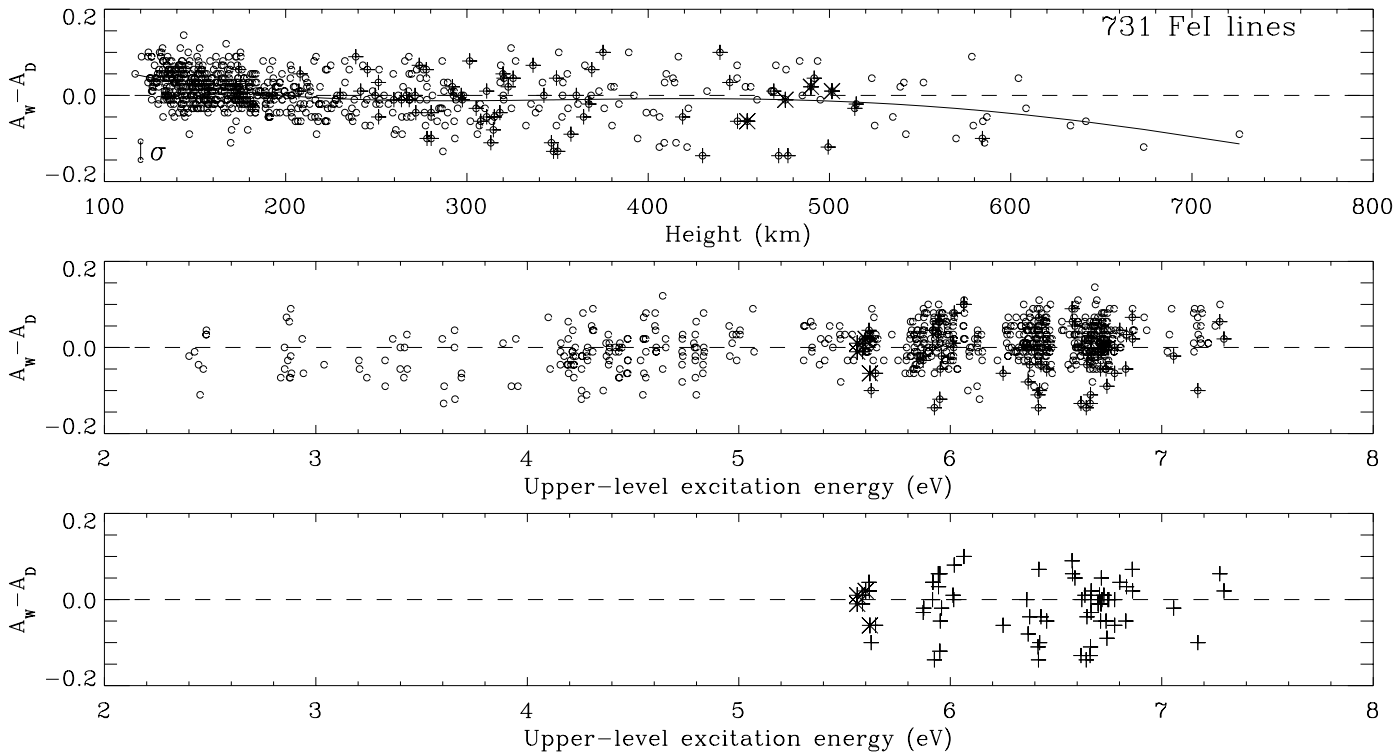

Fig. 8. Difference between line-width fits A_W and line-depth fits A_D for 731 Fe I lines, plotted against line-depth formation height h_D (top) and against upper-level excitation energy (lower panels). The curve in the top panel is a least-square third-order polynomial fit. The stars and crosses mark lines with $\log gf > -1$, the stars being lines that are also present in Fig. 7. The bottom panel contains only these large-gf lines for clarity. Results taken from Gurtovenko & Kostik (1989), obtained with $E = 1.3$, height-dependent macroturbulence $v_{\rm ma}$ (about 1.7 km s^{-1}) and height-dependent microturbulence $v_{\rm mi}$ (declining from about 1 km s^{-1} in deep layers to 0.8 km s^{-1} in the upper photosphere)

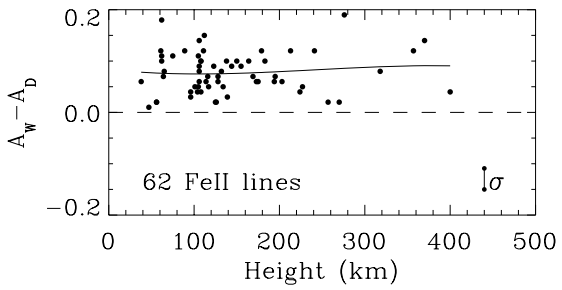

Fig. 9. Difference between line-width fits A_W and line-depth fits A_D plotted against line-depth formation height h_D for 62 Fe II lines. The curve is a least-square third-order polynomial fit. Results taken from Gurtovenko & Kostik (1989), for the same parameters as in Fig. 8

in these Kiev panels (large W and large height); at left, the lines with $h < 200$ km are all part of the cluster with small A_d values (but there are also low–A_D lines formed at larger height). The bulge of the dotted curves in the middle of the panels is mainly produced by the lines of overlap (crosses) and corresponds to the Oxford results.

Thus, the lower six panels of Fig. 7 show that there are indeed selection differences between the Kiel and Oxford line sets that are not apparent from the two top panels. They may be important in causing the observed trend differences. We have therefore made similar dotted fits with the same exclusions in the Kiel panels of Fig. 5 and also marked the large-gf lines in Figs. 5–8 by stars.

The Kiel–Oxford trend differences in Fig. 7 are most outspoken for the top and bottom panels with W and h_D as abscissae, i.e., when plotting A_D against *solar* properties that portray solar line formation. There is no similarly clear-cut trend difference between the Kiel and Oxford panels with E.P. and $\log gf$ as abscissae, i.e., when plotting A_D against *laboratory* properties that may affect gf measurement. The low A_D values for the Kiel lines are spread over both E.P. and $\log gf$, but the larger Kiel A_D values are clustered into two narrow bins of excitation energy, near E.P. = 3.6 eV for the five large-gf lines (stars) and near E.P. = 2.3 eV for the lines of overlap (crosses). The latter cluster seems to reincarnate the Oxford 2.2 eV anomaly issue, but the crosses in the Oxford panel at right do not deviate significantly in fitted A_D from the other Oxford lines.

We conclude from these plots that the Kiel and Oxford data agree for the lines of overlap (as indeed do their gf measurements from Hannover and Kiel), and that the worrisome trends seen in the Kiel panels of Figs. 5 and 7 are dominated by types of line not represented in the Oxford sample. In the remainder of this section we therefore discuss whether solar

line formation processes may separate the different types of Kiel lines in A_D behavior.

NLTE ionization. The pioneering Fe I NLTE analysis by Lites (Lites 1972, Athay & Lites 1972) demonstrated that at heights around the solar temperature minimum ($h \approx 500$ km) most Fe I lines suffer from NLTE overionization which may reduce their opacity compared with LTE estimates by as much as 0.3 dex. The amount is model dependent; appreciable corrections are needed for ultraviolet overionization wherever the photospheric temperature gradient is steep (see Rutten 1988, 1990 for more explanation).

This pitfall of Fe I line formation may be evaded to considerable extent by adopting the model photosphere of Holweger & Müller (1974). We have earlier shown (Rutten & Kostik 1982, 1988) that it hides such Fe I NLTE ionization departures, when present, in its temperature structure with remarkable success. Demonstrations are given in Fig. 3 of Rutten & Zwaan (1983) and in Fig. 2 of Rutten (1988b). Figure 8 represents another one.

The Holweger-Müller model is the ubiquitous choice of abundance determiners for this reason; it was also employed at Kiel and Oxford. Therefore, the Kiel, Oxford and Kiev abundance determinations discussed here should not suffer much from NLTE departures in the actual solar Fe I ionization balance. In any case, since lines with about the same height of formation suffer approximately the same loss of opacity, Fe I ionization effects (or deficiencies in their implicit correction by the model atmosphere) cannot explain the trend difference between the two bottom panels of Fig. 7.

NLTE excitation. Departures from LTE in the Fe I excitation balance between the upper and lower levels of observed lines affect, when present, the line source function rather than the line opacity. As pointed out by Rutten & Kostik (1982) and Rutten (1988, 1990), the *only* Fe I lines in the visible which may possess significant NLTE source function departures are the lines with the highest transition probability in a given bin of upper-level excitation energy. These lines suffer photon losses, whereas the weaker lines in the same upper-excitation class are kept thermalized at their deeper height of formation by these strongest lines per class. The higher the upper-level excitation and the larger the transition probability, the larger is the expected NLTE excitation deficit in the line (until one reaches the Rydberg regime, cf. Rutten & Carlsson 1994).

Therefore, the prime suspects for line source function departures are the Fe I lines with large transition probability. This is the reason that we have marked all lines with $\log gf > -1$ in Figs. 5—8. The large-gf lines marked by stars in the Kiel panels of Fig. 5 and Fig. 7 indeed deviate markedly; they produce significantly larger A_W values (for $E = 1.2$) and larger A_D values (for any E) than the other lines. The sign of this difference fits with the effect of NLTE photon losses since these lower the line source function and make the observed line deeper than the LTE prediction. A larger abundance value is then required to fit their depth and area from LTE modeling.

Thus, the Kiel lines marked by stars may produce their overly large A_W and A_D abundance values from solar NLTE photon losses. However, one than expects that the line depth fits A_D should be more affected than the equivalent width fits A_W, because the line center originates in higher layers than the rest of the line. As a result, such lines should drop below the average fit in $A_W - A_D$ plots as Figs. 6 and Fig. 8 (or below the zero line when the model corrects properly for overionization if present) show. This is not the case, however. The stars in Figs. 6 and the stars and crosses in Fig. 8 do not deviate differentially from the other lines. Also, there is no significant difference between lines of different upper-level excitation energy (including the stars) in the lower panels of Fig. 8.

We conclude that NLTE line excitation may play a role in producing large abundance fits for the large-gf Kiel lines — but not a clear-cut one.

Inhomogeneities. The final selection effect to discuss is difference in sensitivity to inhomogeneities. The worst deviations from plane-parallel time-independent stratification that are suffered by Fe I lines in the visible are caused by the solar granulation in the deep photosphere. In the middle photosphere ($h \approx 300$ km) the convective overshoot is less vigorous and the spectral line response to small-scale inhomogeneity is smoothed by increased lateral radiative cross-talk from neighboring regions. Around $h = 500$ km the major structuring agent is the acoustic five-to-three minute oscillation (Lites et al. 1993), of which the effects on spatially-averaged lines are fairly well described with the turbulence parameters; this layer actually represents the smoothest shell in the solar atmosphere (Rutten 1990b). The violent hydrodynamical disturbances of the chromosphere above it, which totally upset the paradigm of a mean atmosphere in hydrostatic equilibrium (Carlsson & Stein 1994), are not felt at all by Fe I lines in the visible. Thus, effects from inhomogeneities may be expected especially for those Fe I lines in our samples that form the deepest.

The cluster of Kiel lines with $h_D < 200$ km in the bottom-left panel of Fig. 7 produce low A_W and A_D values. Since there are no lines formed below $h = 200$ km in the Oxford set, the trend difference may be influenced also by this selection difference and may be imposed by line formation conditions in the solar granulaton rather than in the Hannover laboratory. However, most lines formed at $200 < h_D < 300$ km are also significantly lower in the Kiel panel than in the Oxford panel. In addition, there is no significant A_D difference between lines at low and high excitation as one might expect from corresponding difference in response characteristics if convective inhomogeneity is important. Comparison with the second Kiel panel shows that the cluster for $h_D < 200$ km consists of lines that range widely in excitation energy. The conclusion is again that a solar selection effect may be at work, but not in clear-cut fashion.

Fe II lines. A final item to discuss is the use of Fe II lines in abundance determination. This paper has been restricted to Fe I lines as diagnostics, but more trust is generally placed in using Fe II lines because iron is predominantly ionized in the solar atmosphere. The often-stated fact that Fe II lines therefore do not suffer from NLTE overionization is correct, but Fe II is not free from other NLTE problems. The optical pumping identified in Fe II by Cram et al. (1980) affects many subordinate Fe II lines in the optical part of the spectrum, again especially wherever the photospheric temperature gradient is steep. The effect of this pumping on source function behavior increases rapidly to the infrared; adopting LTE for Fe II lines is especially dangerous at longer wavelengths (see Fig. 2 of Rutten & Kostik 1982 and the explanation in Rutten 1988a).

Figure 9 confirms that Fe II lines do not necessarily obey the assumptions of classical abundance determination. The Fe II $A_W - A_D$ differences determined by Gurtovenko & Kostik (1989) have a mean value that is significantly offset from zero. The offset implies that the Fe II lines in the visible solar spectrum are not correctly reproduced by adopting the modeling assumptions that reproduce the Fe I lines well.

7. Conclusion

We have clarified the various discrepancies to some extent. The Kiev–Oxford code discrepancy has been explained. The Oxford 2.2 eV anomaly has largely disappeared. However, the Kiel–Oxford discrepancy still remains. It is partially due to significant differences in the equivalent width determinations, but most of it seems due to the presence of systematic offsets in the Hannover *gf* values that produce the trends portrayed in Fig. 5 and Fig. 7. However, solar line formation effects that enter the Kiel–Oxford comparison for categories of lines not represented in the Oxford data cannot be excluded. In particular, NLTE photon losses may affect the large-*gf* Kiel lines and the solar granulation may affect the deepest-formed Kiel lines.

Thus, our Kiel–Oxford comparisons support the conclusion of Grevesse & Noels (1993) that the spread in solar iron abundances determined from solar Fe I lines remains dominated by the uncertainties of their *gf* values. In additon, we found that within the narrow constraints of classical modeling, the collisional damping remains a major uncertainty. Our results above show that the ad-hoc enhancement factor E sets the derived abundance result as well as the patterns in the variations around the mean to an undesirable extent.

More in general, the E parameter is suspect because it may represent the neglect of solar inhomogeneities, in particular the granulation and the attendant NLTE line formation, more than it represents actual deficiencies in the atomic physics of impact broadening (Nordlund 1984, Bruls & Rutten 1992). Detailed NLTE radiation-hydrodynamics modeling is therefore required. The estimation of NLTE effects from the Holweger-Müller model or the computation of line profiles from a granulation simulation assuming LTE represent inconsistent and non-definitive tests.

It is a distinct possibility that eventually, detailed three-dimensional time-dependent numerical simulation of the solar atmosphere including detailed NLTE radiative transfer and employing precise transition probabilities will produce a definitive iron abundance value that actually equals the current result of classical modeling (the Sun being nice rather than nasty, cf. Rutten 1990a, 1990b), but performing such detailed simulation is the *only* venue proving so. Sofar, such verification has been out of reach due to lack of computer power and atomic physics data, but the currently available workstations and atomic databases bring it into reach (cf. Gustafsson & Jørgensen 1994).

Finally — what is the solar iron abundance? The nine lines of overlap between our Kiel and Oxford selections that are marked by crosses in Fig. 7 produce $A_D = 7.60 \pm 0.04$ and $A_W = 7.61 \pm 0.03$ from the Kiel *gf* values and $A_D = 7.62 \pm 0.04$ and $A_W = 7.63 \pm 0.04$ from the Oxford *gf* values when we fit our own W and D measurements for these lines with microturbulence $v_{\rm mi} = 0.9$ km s^{-1}, macroturbulence $v_{\rm ma} = 1.6$ km s^{-1} and damping enhancement factor $E = 1.45$. The latter was again selected by the "neck" method of Fig. 4 to give the smallest spread from the nine abundances A_W per line. These results seem to confirm the "high" value rather than the "low" one. However, they do not have much significance if the trend differences between the remaining lines are not explained. We therefore see no compelling reason to reject equality between the solar and the meteorite iron abundance at present. The moral of this paper is that such equality isn't proven yet either, and that it won't be proven as long as the input oscillator strengths remain disputable and classical abundance determination is not validated by more realistic modeling. The last word on the photospheric iron abundance is *not* in.

Acknowledgements. We thank V. B. Kolluch for help with the computations and V. A. Sheminova and A. S. Gadun for the use of their line synthesis code. We are much indebted to the Nederlands Organization for Scientific Research (NWO) for a generous grant covering Kiev-to-Utrecht travel costs as well as the acquisition of a modern computer system at Kiev. We thank the referee, Dr. N. Grevesse, for his careful and worthwhile comments as well as for prompting the editor to get us the manuscripts of Blackwell et al. (1995) and Holweger et al. (1995).

References

Allen, C. W. 1976, Astrophysical Quantities, Athlone Press, Univ. London

Anders, E., Grevesse, N. 1989, Geochim. Cosmochim. Acta, 53, 197

Athay, R. G., Lites, B. W. 1972, ApJ, 176, 809

Babii, B. T., Kovalchuk, M. M. 1988, Solnechnye Dannye, 5, 88

Bard, A., Kock, A., Kock, M. 1991, A&A, 248, 315

Bates, D. R., Damgaard, A. 1949, Phil. Trans. R. Soc. London, 242, 101

Biémont, E., Baudoux, M., Kurucz, R. L., Ansbacher, W., Pinnington, E. H. 1991, A&A, 249, 539

Blackwell, D., Lynas-Gray, A., Smith, G. 1995, A&A, in press

Blackwell, D. E., Booth, A., Haddock, D. J., Menon, S. L. R., Petford, A. D., Leggett, S. K. 1986, MNRAS, 220, 549

Blackwell, D. E., Booth, A. J., Petford, A. D. 1984, A&A, 132, 236

Blackwell, D. E., Petford, A. D., Shallis, M. J. 1979, MNRAS, 186, 657

Blackwell, D. E., Petford, A. D., Shallis, M. J., Simmons, G. J. 1980, MNRAS, 191, 445

Blackwell, D. E., Petford, A. D., Shallis, M. J., Simmons, G. J. 1982a, MNRAS, 199, 43

Blackwell, D. E., Petford, A. D., Simmons, G. J. 1982b, MNRAS, 201, 595

Blackwell, D. E., Shallis, M. J., Simmons, G. J. 1982c, MNRAS, 199, 33

Booth, A. J. 1989, A&A, 208, 287

Bruls, J. H. M. J., Rutten, R. J. 1992, A&A, 265, 257

Bruls, J. H. M. J., Rutten, R. J., Shchukina, N. G. 1992, A&A, 265, 237

Carlsson, M., Rutten, R. J., Bruls, J. H. M. J., Shchukina, N. G. 1994, A&A, 288, 860

Carlsson, M., Rutten, R. J., Shchukina, N. G. 1992, A&A, 253, 567

Carlsson, M., Stein, R. F. 1994, in M. Carlsson (ed.), Chromospheric Dynamics, Proc. Miniworkshop, Inst. Theor. Astrophys., Oslo, p. 47
Cram, L. E., Rutten, R. J., Lites, B. W. 1980, ApJ, 241, 374
Delbouille, L., Neven, L., Roland, G. 1973, Photometric atlas of the solar spectrum from $\lambda 3\,000$ to $\lambda 10\,000$, Institut d'Astrophysique de l'Université de Liège, Liège, Belgium
Gadun, A. S., Sheminova, V. A. 1988, SPANSAT: Program for calculating absorption line profiles in stellar atmospheres in LTE approximation, Preprint No. ITF-88-87P, Inst. Theor. Physics Ukrainian Acad. Sciences
Garz, T., Heise, H., Richter, J. 1970, A&A, 9, 296
Grevesse, N., Noels, A. 1993, Phys. Scripta, T47, 133
Gurtovenko, E. A., Kondrashova, N. N. 1980, Solar Phys., 68, 17
Gurtovenko, E. A., Kostik, R. I. 1981, A&AS, 46, 239
Gurtovenko, E. A., Kostik, R. I. 1982, A&AS, 47, 193
Gurtovenko, E. A., Kostik, R. I. 1989, Fraunhofer Spectrum and the System of Solar Oscillator Strengths, Naukova Dumka, Kiev
Gurtovenko, E. A., Kostik, R. I., Rutten, R. J. 1990, in J.-O. Stenflo (ed.), The Solar Photosphere: Structure, Convection and Magnetic Fields, IAU Symp. 138 (Kiev), Kluwer, Dordrecht, p. 35
Gurtovenko, E. A., Sheminova, V. A. 1988, Kinematika i Fizika Nebesnich Tel., 4, 18
Gustafsson, B., Jørgensen, U. G. 1994, A&AR, 6, 19
Halenka, J., Grabowski, B. 1984, A&AS, 57, 43
Hannaford, P., Lowe, R. M., Grevesse, N., Noels, A. 1992, A&A, 259, 301
Holweger, H. 1970, A&A, 4, 11
Holweger, H., Bard, A., Kock, A., Kock, M. 1991, A&A, 249, 545
Holweger, H., Gelsen, M., Ruland, F. 1978, A&A, 70, 537
Holweger, H., Heise, C., Kock, M. 1990, A&A, 232, 510
Holweger, H., Kock, M., Bard, A. 1995, A&A, in press
Holweger, H., Müller, E. A. 1974, Solar Phys., 39, 19
Irwin, A. 1981, ApJS, 45, 621
Kipper, T. 1987, Tartu Astrof. Obs. Publ., 52, 281
Kostik, R. I. 1982, Solar Phys., 78, 39
Kurucz, R. 1974, Solar Phys., 34, 17
Lites, B. W. 1972, Observation and Analysis of the Solar Neutral Iron Spectrum, NCAR Cooperative Thesis No. 28, High Altitude Observatory, Boulder
Lites, B. W., Rutten, R. J., Kalkofen, W. 1993, ApJ, 414, 345
Magain, P. 1984, A&A, 132, 208
Mihalas, D. 1978, Stellar Atmospheres, W. H. Freeman and Co., San Francisco (second edition)
Milford, P. N., O'Mara, B. J., Ross, J. E. 1994, A&A, 292, 276
Moore, C. E., Minnaert, M. G. J., Houtgast, J. 1966, The Solar Spectrum 2935 Å to 8770 Å. Second Revision of Rowland's Preliminary Table of Solar Spectrum Wavelengths, NBS Monograph 61, National Bureau of Standards, Washington
Nordlund, Å. 1984, in S. L. Keil (ed.), Small-Scale Dynamical Processes in Quiet Stellar Atmospheres, National Solar Observatory Summer Conference, Sacramento Peak Observatory, Sunspot, p. 181
Pauls, U., Grevesse, N., Huber, M. C. E. 1990, A&A, 231, 536
Rutten, R. J. 1988a, in R. Viotti, A. Vittone, M. Friedjung (eds.), Physics of Formation of FeII Lines Outside LTE, IAU Coll94, Reidel, Dordrecht, p. 185
Rutten, R. J. 1988b, in G. Cayrel de Strobel, M. Spite (eds.), The Impact of Very High S/N Spectroscopy on Stellar Physics, IAU Symp. 132, Reidel, Dordrecht, p. 367
Rutten, R. J. 1990a, in J.-O. Stenflo (ed.), Solar Photosphere: Structure, Convection and Magnetic Fields, IAU Symp. 138 (Kiev), Kluwer, Dordrecht, p. 501
Rutten, R. J. 1990b, in G. Wallerstein (ed.), Cool Stars, Stellar Systems and the Sun, Proc. Sixth Cambridge Workshop, Astron. Soc. Pac. Conf. Series 9, p. 91
Rutten, R. J., Carlsson, M. 1994, in D. M. Rabin, J. T. Jefferies, C. Lindsey (eds.), Infrared Solar Physics, Proc. Symp. 154 IAU (Tucson), Kluwer, Dordrecht, p. 309
Rutten, R. J., Kostik, R. I. 1982, A&A, 115, 104
Rutten, R. J., Kostik, R. I. 1988, in R. Viotti, A. Vittone, M. Friedjung (eds.), Physics of Formation of FeII Lines Outside LTE, IAU Coll. 94, Reidel, Dordrecht, p. 83
Rutten, R. J., van der Zalm, E. B. J. 1984, A&AS, 55, 143
Rutten, R. J., Zwaan, C. 1983, A&A, 117, 21
Shchukina, N. G., Shcherbina, T. G., Rutten, R. J. 1990, in J.-O. Stenflo (ed.), Solar Photosphere: Structure, Convection and Magnetic Fields, IAU Symp. 138 (Kiev), Kluwer, Dordrecht, p. 29
Thévenin, F. 1989, A&AS, 77, 137
Unsöld, A. 1955, Physik der Sternatmosphären, Springer Verlag, Berlin (second edition)
Vernazza, J. E., Avrett, E. H., Loeser, R. 1976, ApJS, 30, 1
Warner, B. 1969, Observatory, 89, 11

This article was processed by the author using Springer-Verlag LaTeX A&A style file 1990.